Geophys. J. R. astr. Soc. (1982) **68**, 499–530

Aftershock tectonics of the 1978 Tabas-e-Golshan (Iran) earthquake sequence: a documented active 'thin- and thick-skinned tectonic' case

Manuel Berberian *Department of Earth Sciences, Bullard Laboratories, University of Cambridge, Madingley Rise, Madingley Road, Cambridge CB3 0EZ*

Received 1981 June 15; in original form 1981 March 11

Summary. In this study a locally recorded aftershock sequence of the 1978 Tabas-e-Golshan earthquake (M_s = 7.4) was accurately located. Out of 1560 located events, 329 best-located aftershocks passed a strict quality criterion. These well-located aftershocks, which have uncertainties in epicentre and in focal depth of about 1 and 2 km respectively, together with the well-constrained focal mechanisms, provided a detailed picture of active continental deformation during an aftershock sequence.

Almost all aftershocks follow very closely the pattern of the earthquake faults at the surface and lie in the hanging-wall block of the active fault. The hypocentres occurred mainly at depths less than 23 km with a high concentration of seismic activity between 8–14 km depth. The aftershocks clearly demonstrate an active imbricate listric thrust system with fault planes flattening into a basement decollement zone, and the reactivation of different basement reverse faults in response to a considerable amount of shortening of the top sedimentary cover. The sense of motion was almost universally thrusting and the aftershocks shared the same tectonic causes as the main shock.

The study indicates that the development of the young fold-thrust mountain belts necessarily involves basement shortening (thin- and thick-skinned tectonics) and that the 'frontal reverse faults' in young active fold-thrust mountain belts are the most seismically active faults. Geological and seismic data propose that the active frontal reverse fault systems are possibly reactivated old normal faults and may add support to the contention of reversal of fault motion during rethickening of continental crust. The active 'thin- and thick-skinned tectonics' documented in this study may prevail in other young and active fold-thrust mountain belts which are characterized by a thick sequence of telescoped top sedimentary cover over a decollement detachment zone.

1 Introduction

The Tabas-e-Golshan earthquake of magnitude M_s = 7.4 (m_b = 6.4) occurred in east Central Iran on 1978 September 16 at 15.35.56.7 UTC (ISC). The main shock destroyed or

severely damaged about 90 villages, slightly damaged 50 more, and completely demolished the town of the Tabas where 85 per cent of the population was killed. In total, the shock killed over 20 000 people, injured thousands, and destroyed over 15 000 housing units and 30 qanats (Berberian 1979a). Multiple frontal thrust faulting at the surface and bedding-plane slips of thrust mechanism in the hanging-wall block occurred along a major existing but hitherto unrecognized Quaternary fault, the 'Tabas Fault' (Berberian 1979b). Three small magnitude earthquakes had occurred on the same fault system but there is no historical record of damage, at least for the last eleven centuries and no perceptible fore-shocks occurred in the last 12 months preceding the main shock. The surface ruptures associated with the 1978 main shock extended for about 85 km in ten discontinuous thrust segments with a NNW–SSE trend. The fault segments were separated by gaps in the surface ruptures in a complicated pattern along curved lines (Berberian 1979b). The Tabas active fault was a thrust at the base of a series of low foothills made up to Neogene clay deposits which separate the Shotori fold-thrust mountain belt (in the east) from the Tabas compressional depression (in the west; Fig. 1). The minimum vertical uplift and total slip were about 150 and 300 cm, respectively (Berberian 1979b). Multiple imbricate thrust faults along the main fault zone (ranging from 1 to about 30 m width), together with highly deformed Neogene sediments in the hanging-wall block with extensive development of

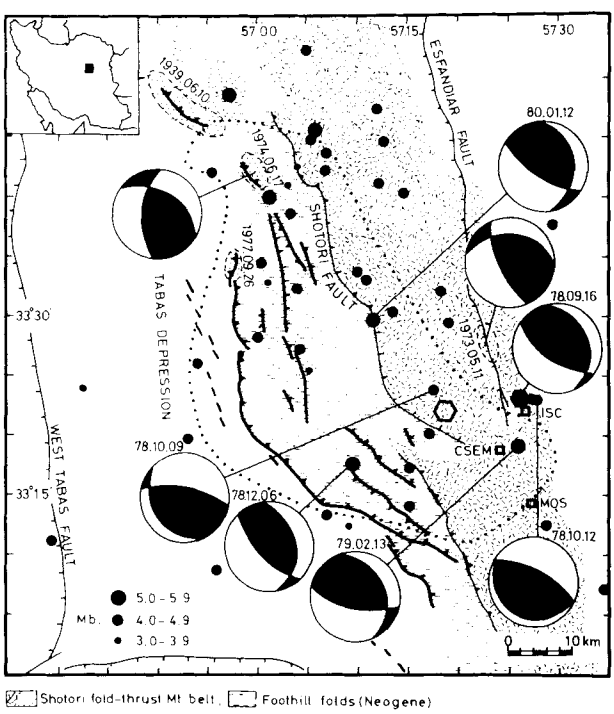

Figure 1. Epicentres of the main shock (solid hexagon) and teleseismically located aftershocks (NEIS) of magnitude M_b = 3.0 and greater, of the Tabas-e-Golshan earthquake sequence for 16 months of activity, 1978 September 16 to 1980. The relocated position of the 1978 main shock is marked by a blank hexagon. ISC, CSEM and MOS locations for the main shock are shown by squares. Epicentral areas of pre-1978 earthquakes are stippled. Surface ruptures associated with the 1978.09.16 earthquake are shown by solid lines (after Berberian 1979b). For first motion polarity observation of the fault-plane solutions (equal-area projection of the lower focal hemisphere) see Figs 2 and 12. The dotted line indicates the approximate aftershock zone revealed by the best-located locally recorded aftershocks (see Fig. 6). Mercator projection.

bedding-plane slips of thrust mechanism (over a broad zone of about 8 km width), all indicate a 'high internal deformation' and an 'increased seismic shaking' of the hanging-wall block. The reverberation of seismic energy between the fault plane and the free surface in the hanging-wall block could be responsible for this intense shaking (Nason 1973). Very strong shaking and deformation of the hanging-wall were also observed during the 1964 Alaskan earthquake (Plafker 1972) and the 1971 San Fernando earthquake (Nason 1973).

Epicentral zones of the twentieth century earthquakes along the Tabas active fault show a southward shifting of seismicity along this active fault (Fig. 1) to the nucleation zone of the 1978 earthquake and the preparation of the region for the 1978 earthquake associated with 85 km of surface faulting (Berberian 1979b). The north-western segment of the Tabas active fault is segmented by longer barriers and has been the site of three low to moderate magnitude earthquakes (Fig. 1). Presumably the barriers could have acted as stress concentrations causing the migration and progression of the earthquakes southwards along the fault line.

Despite 85 km of curved multiple thrust faulting at the surface with a NNW–SSE trend, only 40 km of a straight fault with a trend of N10°W was mapped by Mohajer-Ashjai & Nowroozi (1979). A preliminary map given by Sharp & Orsini (1978) shows 60 km of the major ruptures and does not cover all the surface ruptures developed during the main shock. A well-constrained fault plane solution of the main shock, based on long-period polarity observations (Figs 1 and 2), shows ENE-dipping pure thrust faulting in the source region on a fault with a NNW trend (Berberian *et al.* 1979). The mechanism and fault geometry of this solution agree with the mapped surface ruptures. However, the fault plane solution presented by Akasheh & Eshghi (1980/81) shows a pure right-lateral strike-slip mechanism with a N–S trend for the main shock. This inconsistency is due to the fact that the authors have used reported polarity readings of mainly short-period and a few long-period stations. It is known that short-period data are sensitive to the detailed behaviour of the source and to the velocity structure at the source and at the receiver sites and therefore do not generally provide a reliable focal mechanism solution.

Although the main shock of 1978.09.16 took place without any teleseismically recorded foreshock, it was followed by considerable aftershock activity which lasted for 16 months (Fig. 1). The last teleseismically located aftershock was on 1980 January 12, and since then no teleseismic aftershock has been recorded by the international seismic networks (NEIS).

The Tabas-e-Golshan earthquake of 1978.09.16 provided an opportunity to record and study its aftershock sequence. The study of such sequences provides an important constraint on the present-day continental deformation of the Iranian plateau. The recording period started on 1978 September 27 and ended on 1978 October 28 (Fig. 3). A total of 300 seismograms, containing more than 60 000 *P*-arrivals in total, were obtained during this time interval. The field-work lasted 40 days during which the surface ruptures associated with the main shock and the epicentral area were mapped and studied in detail.

2 Recording instrument and procedure

The aftershock recording started 12 days after the main shock and lasted for about 30 days (Fig. 3). The instruments used were five portable Sprengnether MEQ-800 and four Lamont seismographs with large drums with Mark Product L-4C 1-Hz and Willmore MKII vertical component seismometers. The time was maintained by an internal crystal clock and the radio time marks (usually the Moscow station) were put on the records to check the clock drift. Care was taken to put the radio timing marks on the beginning and the end of each record. Clock drifts were marked on each record as time corrections; it was observed that the drift was always less than 0.05 s for a 48 hr period. Time corrections were linearly inter-

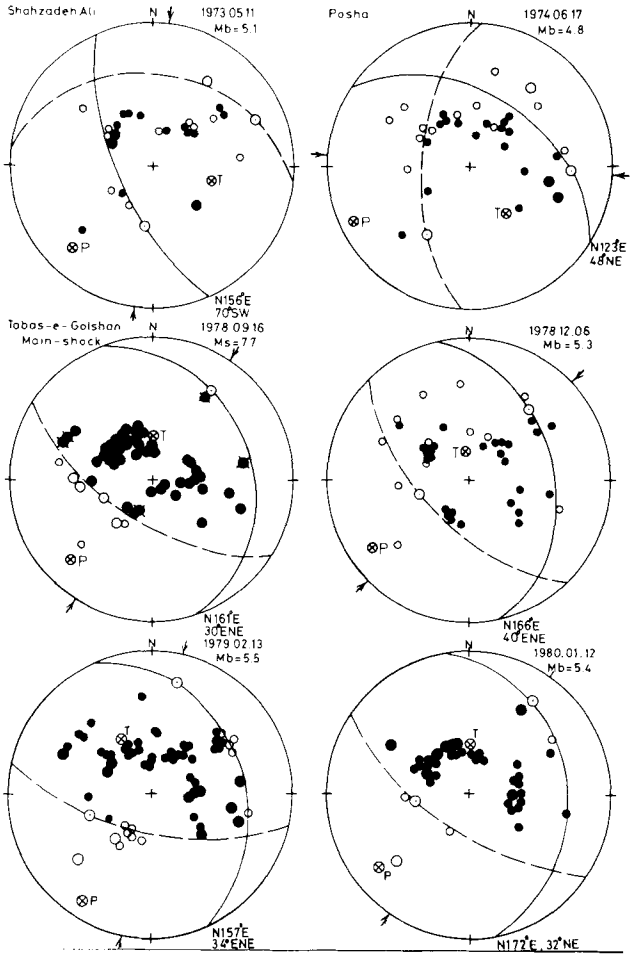

Figure 2. First motion data and their focal mechanism fits (equal-area projection of the lower focal hemisphere) of the large magnitude earthquakes along the Tabas active fault and the Esfandiar fault (only for the 1973.05.11 event). For locations see Fig. 1. Solid circles are compressions and open circles dilatations. Long-period polarity observations are shown as large circles and short-period data as small circles. For the 1978.12.06 event the long-period polarity was disturbed due to the dominant surface waves from the Kuril island earthquake. Long-period data were not complete for the 1979.02.13 and the 1980.01.12 aftershocks, therefore both long- and short-period data were used. The nodal plane drawn as a solid line is the inferred plane of faulting. The foci are taken to be in the crust with a *P*-wave velocity of 6.8 km s^{-1}. The horizontal projections of the slip vectors are shown by lines with arrows. *T* – tension axis, *P* – pressure axis.

polated on each record and were added to each earthquake arrival time in the location programme. The *P*- and *S*-wave arrival times, the maximum amplitude and the end of the wavetrain of each shock were digitized on a high resolution digitizing table. The digitized data were transformed to arrival times and signal duration data for each earthquake. In general the *P*-wave arrival times could be measured with uncertainties of 0.1 s and the *S*-wave arrival times are on average uncertain by about 0.3 s. Earthquake locations were determined using the HYPO-71 computer program (Lee & Lahr 1975). Since the *S*-wave arrivals were less reliable, they were given 25 per cent (of the *P*-weight) in the computer location program. A time correction for the altitude difference was calculated by dividing the altitude difference of each station from the lowest station by the *P*-wave velocity of the top

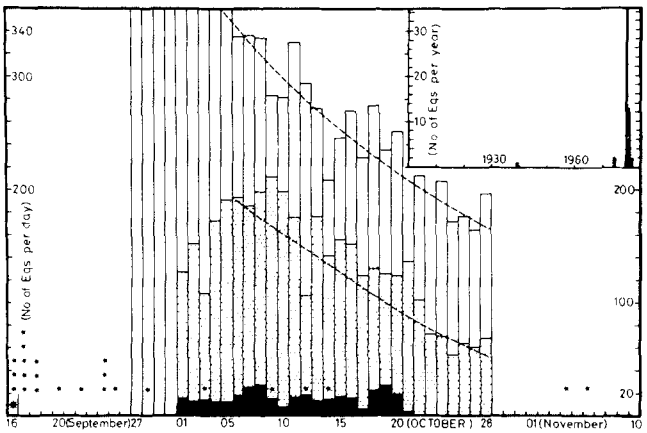

Figure 3. Daily frequency of occurrence of the Tabas aftershocks detected by the local portable network. Blank histograms: aftershocks recorded by at least two instruments, dotted: recorded by at least four stations, and black: best-located aftershocks which passed all the quality criteria (at least with 5*P*- and 3*S*-readings, errors in hypocentre and epicentre < 2 km, rms < 0.2 s). Asterisks are teleseismically recorded aftershocks by NEIS. Broken lines show the overall decay of the aftershock activity. *Inset top right:* number of teleseismically detected earthquakes per year along the Tabas active fault during the twentieth century. The relative seismic quiescence along the Tabas fault prior to the 1978 earthquake ($M_S = 7.4$) is noticeable. Large magnitude aftershocks lasted for 16 months and the last teleseismically recorded event was on 1980 January 12.

layer. This time correction plus the daily time correction for each station were added to the earthquake arrival times. The magnitude of the aftershocks were estimated from the duration of the signal using the formula:

$$M_l = C + 2 \log T + 0.0035D$$

where:

C = constant for each station,
T = duration signal in seconds,
D = epicentral distance in kilometres (Lee & Lahr 1975).

The local magnitudes (M_l) for four large aftershocks were determined by the Mashhad station and were used to calibrate the constant C for each station of the local network.

3 Velocity structure obtained using real data

The knowledge of the crustal structure in Iran is limited and the velocity structure in the Tabas–Shotori area is not known in detail. There are various estimates of the average crustal thickness in Iran along a line passing through the Tabas area (from the Shiraz WWSSN station to Mashhad). These are: about 50 km (Moazami-Goudarzi 1974; Akasheh 1975), larger than 35 km (Arkhangl'skaya, Gergaui & Sheckov 1974), 55 km (McCowan 1978) and 45 km (Peive & Yanshin 1979). These estimates are in agreement with the recent results of surface wave studies which suggest a crustal thickness of 44 km for this area (I. Asudeh 1980, private communication).

In order to define a more detailed velocity structure for the Tabas region the value for the ratio of the *P*- and *S*-wave velocities was estimated using real data. Since the HYPO-71 program (Lee & Lahr 1975) uses a constant V_p/V_s ratio for all depths, 50 well-recorded events with *S*-readings were chosen to construct the Wadati diagram. The V_p/V_s estimate was found from the gradient of the plot of the $(S-P)$ travel time versus the *P*-travel time. The average

ratio V_p/V_s value was found to be about 1.85 and was then used for all locations. This value was confirmed when the earthquakes were relocated by changing the V_p/V_s values from 1.60 to 1.90 using a single layer model over a half space. The result of this trial supported the value obtained from the Wadati diagram. The average value obtained seems to be high and may reflect a 'highly fractured' and water-saturated nature for the area where the seismic waves were propagating (Nur & Simmons 1969; Francis, Porter & McGrath 1977).

Since no seismic refraction survey has been carried out in the Tabas area or the nearby regions, the simplest model composed of a single homogeneous layer of crust of thickness 44 km over a half space was initially chosen. Locations obtained from 119 well-recorded earthquakes (with at least 5*P*- and 2*S*-readings) using a single layer model and *P*-wave velocities ranging between 4.8 and 6.4 km s^{-1} were studied. The *P*-velocity which minimized the root mean square (rms) residuals of the locations was 5.3 km s^{-1}:

(model I)

V_p (km s^{-1})	Depth (km)
5.3	44.0
8.0	

Travel time–distance curves of *P*-waves for 50 well-recorded and well-located earthquakes (with rms < 0.2 s, focal depth range = 5–16 km, located with the single layer model) were then constructed which gave a *P*-velocity of 5.4 km s^{-1}. The low average *P*-velocity of 5.3 km s^{-1} obtained in this way is not surprising since 60 per cent of the thick sedimentary column of the Tabas–Shotori region is composed of low-velocity rocks (shale and sandstone). Nuttli (1980) has also found a group velocity of 5.4 + 0.2 km s^{-1} for the onset of the P_g-phase of selected earthquakes in Iran.

The HYPO-71 location program obtains the origin time, epicentre and depth by minimizing the sum of the squares of the travel-time residuals. The final hypocentre, therefore, must be at the position where the rms residual is minimum. A group of well-recorded earthquakes was fixed at a certain depth and the location program was made to calculate the best parameters. Plots of rms residuals versus fixed depths for the well-recorded events with *S*-readings, which were located with different fixed depths using single layer model, shows that the model and the network had in general a good depth resolution. The minimum depth values obtained by this analysis correspond to the values calculated by the free solution. However two types of curves, with sharp or broad minima, were observed (because of the space problem and the reviewer's suggestion, figures related to these tests were deleted from the text).

With a single-layer model we assume much of the propagation from source to seismograph is by direct path. Since this may be far from the real Earth, existing geological data of the Tabas–Shotori area were then used to construct a more realistic crustal model. Several combinations were obtained and tried with the well-recorded earthquakes. The minimum rms time residuals were obtained with:

(model II)

V_p (km s^{-1})	Depth (km)
3.00	1.0
5.45	16.0
6.00	44.0
8.00	

As a third alternative, a more complicated model was tested by introducing a continuous velocity increase with depth in the upper part of the crust (Bolt, Kubo & Uhrhammer 1978; Uhrhammer 1980). In this case there will be continuous bending of rays:

(model III)

V_p (km s^{-1})	Depth (km)
4.660	1.0
4.740	2.0
4.820	3.0
4.900	4.0
4.980	5.0
5.060	6.0
5.140	7.0
5.220	8.0
5.300	9.0
5.380	10.0
5.460	11.0
5.540	12.0
5.620	13.0
5.700	14.0
5.780	15.0
5.860	16.0
5.940	18.0
6.100	20.0
6.300	44.0
8.000	

All the aftershocks were then located with these three models and the results compared with each other. It was observed that the epicentral locations were little different for these three models. However, the focal depths varied by 1–2 km. In general the single layer model resulted in larger depths while the three-layered model gave shallower locations by about 1–2 km.

4 Uncertainties in locations and error analysis with synthetic data

To correlate the aftershock activity with the regional structures and identify the active seismic trends, hypocentre locations with the highest possible accuracy are required. The degree of accuracy in locating the events is determined by the adequacy of the assumed crustal model, the geometrical configuration of the network and the precision in time keeping and phase reading. Despite the attempt to construct the best crustal model using the available data (Section 3), it is possible that the obtained models are not adequate even though they produce small residuals, and may introduce significant systematic errors in the hypocentral locations.

The standard errors in the epicentral and hypocentral locations given by the HYPO-71 program for the earthquakes may not represent the actual error limits. A series of tests was therefore carried out with synthetic data (using a test program written by S. W. Roecker and

modified by C. Soufleris) in order to estimate the uncertainties in the aftershock locations due to the configuration of the network, the random noise in the data and the uncertainties in the values of V_p and V_p/V_s used.

4.1 STATION DISTRIBUTION EFFECT

Station distribution plays a critical role in determining whether or not earthquakes can be located accurately by a given network. In order to estimate the effect of the station distribution on the locations, error-free travel-time data were computed for a grid of events covering the epicentral area, both outside and inside the array, and at different depths. These artificial earthquakes were then located with the HYPO-71 location program. Standard errors in origin time, depth, latitude and longitude, with the average standard deviation values for well-located earthquakes of 0.15 s, were computed and contoured. Various combinations of network geometry and numbers of *P*- and *S*-arrivals were considered.

As expected, areas outside the network show large errors. The error contours in different combinations (with or without *S*-readings) show that errors in origin time vary smoothly inside the area covered by the network. Errors in depth are lower near the stations and inside the network and they rapidly increase in areas outside the network. The geometry of the network plays an important role in errors in latitude and longitude. Since the network is elongated along a N–S line, errors in longitude are slightly greater than in latitude. When one *S*-arrival is included, the errors in all four parameters decrease. Further improvement is achieved when 2 to 5 *S*-arrivals are added to the network. The error contours were computed for extreme cases: from $9P$–$0S$-arrivals to $9P$–$5S$-arrivals. The test shows that, with the exception of shallow hypocentres (< 4 km), $5P$- and $3S$-arrivals ensure an accuracy of about 2 km in hypocentre and 1 km in epicentre location for the Tabas aftershock sequence (Fig. 4). If more than $5P$-arrivals are available the same accuracy can be obtained with $2S$-arrivals. Therefore, this criteria is used as a requirement for selecting well-located aftershocks in this study.

4.2 RANDOM NOISE EFFECT

In this test the travel times of events to nine stations were computed using a three-layered model (model II) with a V_p/V_s ratio of 1.85. Random noise of a normal distribution, with zero mean and a standard deviation of 0.1 s for *P*- and 0.3 s for *S*-arrivals was added to the error-free travel times and the events were relocated by the HYPO-71 program. The test was carried out for a varied combination of *P*- and *S*-arrivals. It was observed that the differences in location and hypocentre for the events inside the network were close to the errors predicted by the previous method (see Section 4.1) and close to the errors given by the HYPO-71 location program.

4.3 THE EFFECT OF VARYING THE V_p/V_s RATIO

The hypothetical events were relocated in this test by first adding the random noise and then by varying the ratio of V_p/V_s from 1.65 to 1.90 in order to find the changes in earthquake locations due to this variation. It was observed that the computed location events inside the network differed by less than 2 km from the actual locations. The mislocation error increased for events outside the network.

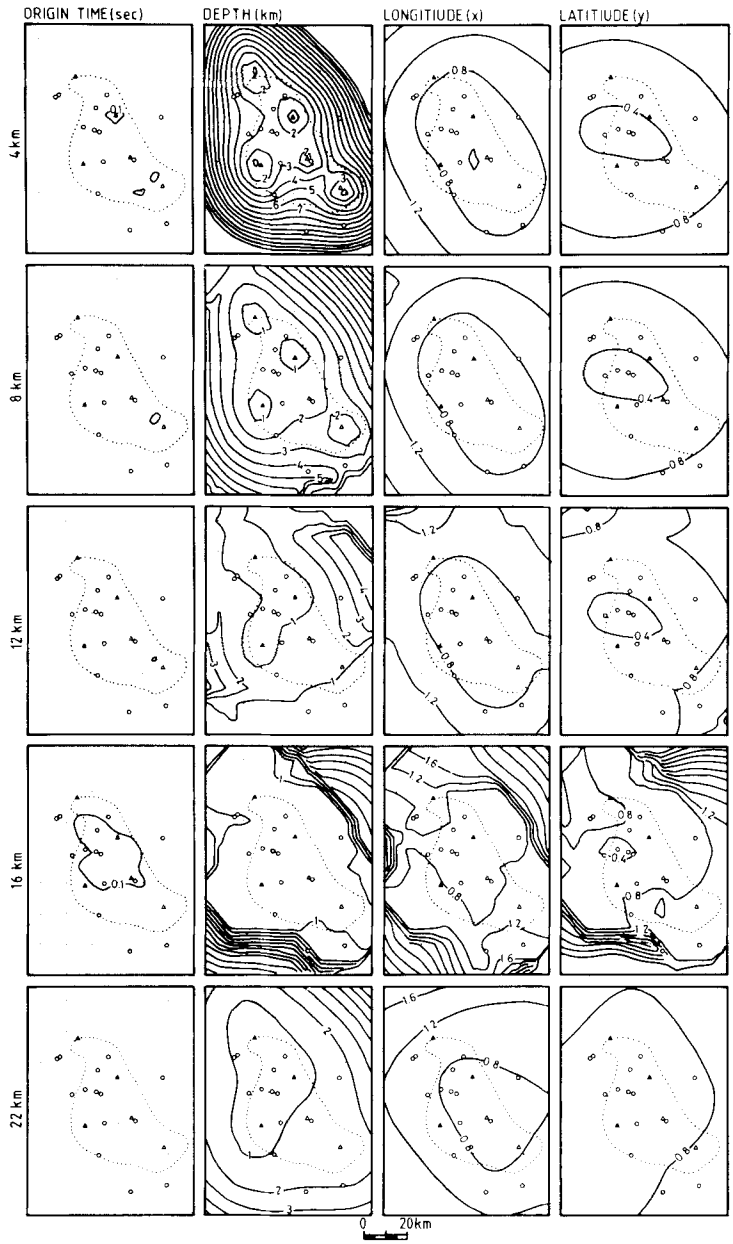

Figure 4. Contours of errors in origin time (in s), depth (in km), longitude (in km) and latitude (in km) for the Tabas network area with 9*P*- and 3*S*-arrivals. The number at the margin of each column of contour maps denotes depth (in km). Stations are shown as triangles (filled if the station reports both *P*- and *S*-arrivals). Stations not included in the test (but which operated during the expedition) are marked with blank circles. The bottom left corner of each contour map is at 33.00'N, 56.40'E and the small dots in between the contours are 8' (i.e. 12.4 × 14.8 km) apart. The station and *P*- and *S*-wave combinations used were not random, but representative of the actually recorded data.

4.4 THE EFFECT OF VARYING V_p

The final test examined the effect of different mean values for the *P*-wave velocity. In this test a homogeneous half space and a constant V_p/V_s ratio were considered with values of V_p

between 4.5 and 6.5 km s^{-1}. In general the events inside the network gave location differences less than 2 km.

From all location tests with real (Section 3) and synthetic data (Section 4) with various network configuration, it is concluded that when 5*P*- and 3*S*-arrivals are used for the events inside the network, the errors in the calculated hypocentre and epicentre are less than 2 and 1 km respectively (except for events shallower than 4 km which could not be located accurately due to the network geometry).

5 Locally recorded aftershocks of the Tabas-e-Golshan earthquake

In the analysis of the spatial distribution of the aftershock hypocentres, 'well-located events' were emphasized. The selection of these events was based on the results of the above location accuracy tests. Such events were defined as those for which:

(1) the focal depth was not held fixed by the location program;
(2) the rms residuals were smaller than 0.20 s;
(3) the errors in epicentre and depth (ERH and ERZ) were less than 2 km;
(4) for which at least 5*P*- and 3*S*-readings were available; and
(5) with at least one station at an epicentral distance smaller than their depth was available.

Out of 1560 located aftershocks (Fig. 5) only 329 events meet these conditions and were chosen for this study (Fig. 6). Almost 560 events satisfied a less stringent quality criteria (5*P*- and 1*S*-reading with rms < 0.30 s, errors in hypocentre and epicentre < 6 km and < 3 km respectively) and show a similar epicentral distribution to those of Figs. 5 and 6. As with the surface ruptures of the earthquake, the aftershock epicentres and hypocentres define a rather complex pattern. The following discussion is based only on the 'high quality locations' (Fig. 6). The other events (Fig. 5) provide only a general view of the aftershock distribution.

5.1 EPICENTRAL PATTERN

The aftershock distribution is 'asymmetrical' with respect to the surface ruptures. They predominantly lie to the east of the mapped surface fault breaks, on thrust planes dipping ENE, indicating an 'intense hanging-wall deformation' (Figs 5 and 6). Aftershocks located by NEIS using teleseismic observations lack depth resolution but show a similar epicentral distribution (Fig. 1). The arcuate-shaped distribution of the aftershock epicentres follows very closely the pattern of the mapped earthquake faults at the surface. The belt of aftershock-slip attains a maximum width of about 38 km at the surface of the hanging-wall block and an average focal depth of about 12 km. The length of the aftershock zone is about 78 km (Fig. 6) and more or less agrees with the surface measurement of the earthquake ruptures (85 km; Berberian 1979b).

5.2 HYPOCENTRAL PATTERN

Majority of the aftershocks, and hence most of the seismic energy released along the Tabas active fault system, came from the depth range of 3–23 km. A series of projections of the best hypocentres, section by section across the earthquake fault, on to vertical planes perpendicular to the surface break are given in Fig. 7 using the single layer model (I). Clearly, sections of this kind require that only hypocentres within a limited and small distance from the cross-section should be projected. Since the zone of the surface ruptures together with the aftershock zone, are arcuate and their trend changes from roughly N–S to NW–SE at about 33.25°N latitude, a composite cross-section is also produced (Fig. 13A).

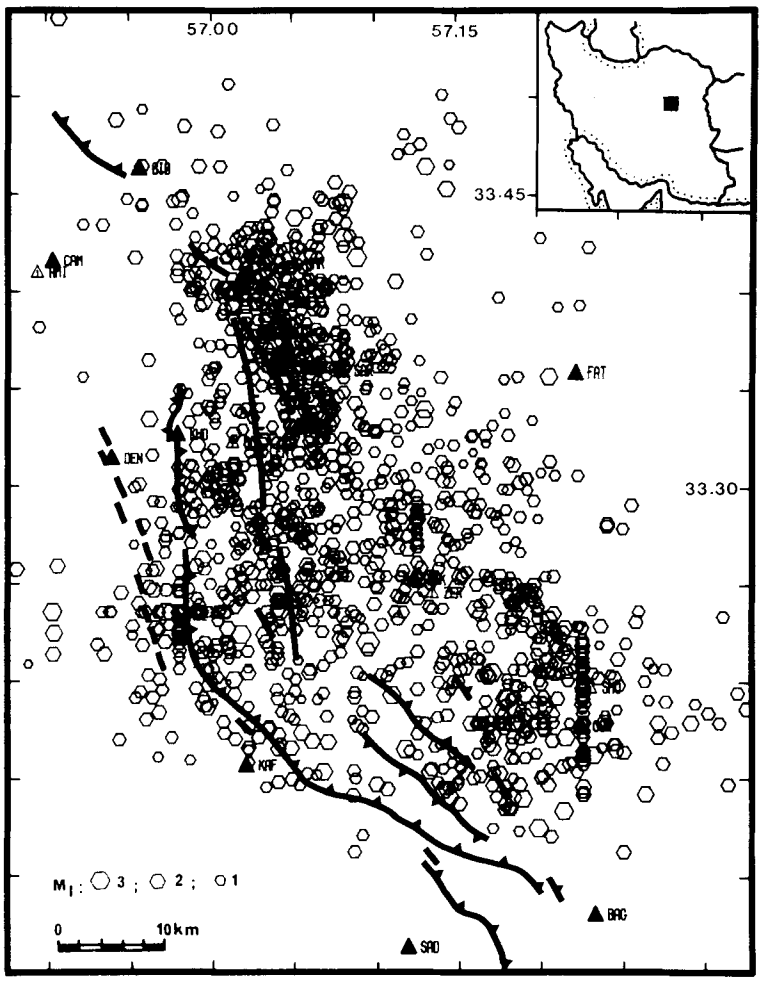

Figure 5. Epicentral distribution of all the located aftershocks (1560 events). Recording stations are shown by filled triangles. The network operated for 30 days. ESP moved to KAF after 11 days and BAG to SAD after three days. Surface earthquake ruptures (Berberian 1979b) are shown by thick lines. Aftershocks were located by a single layer model (I). East–west or north–south linear trends through stations are artifacts of the location procedure. For small and poorly recorded earthquakes the location program cannot resolve their latitude or longitude, and holds it fixed. Mercator projection.

Due to the network geometry, aftershocks with shallow focal depths (< 4 km) usually have large errors in depth (see location error tests). Therefore, no events in this depth range passed the quality criteria. Absence of very shallow events may be a consequence of either a low-strength top zone or the station distribution.

Aftershock hypocentres cover a seismic zone with an average width of about 30 km (ranging from 20 to 40 km) along the 'foothills' of the Shotori mountain (Figs 6 and 7). This is close to the average width of the zone of the surface faulting associated with the main shock (about 30 km). Apparently during the Tabas earthquake sequence a 'zone of about 30 km width' was reactivated from depth to the surface. As with the active surface faulting, the seismic activity was mainly restricted to the 'frontal' parts of the Shotori fold-thrust mountain belt, and it did not propagate to the base and rear of the mountain

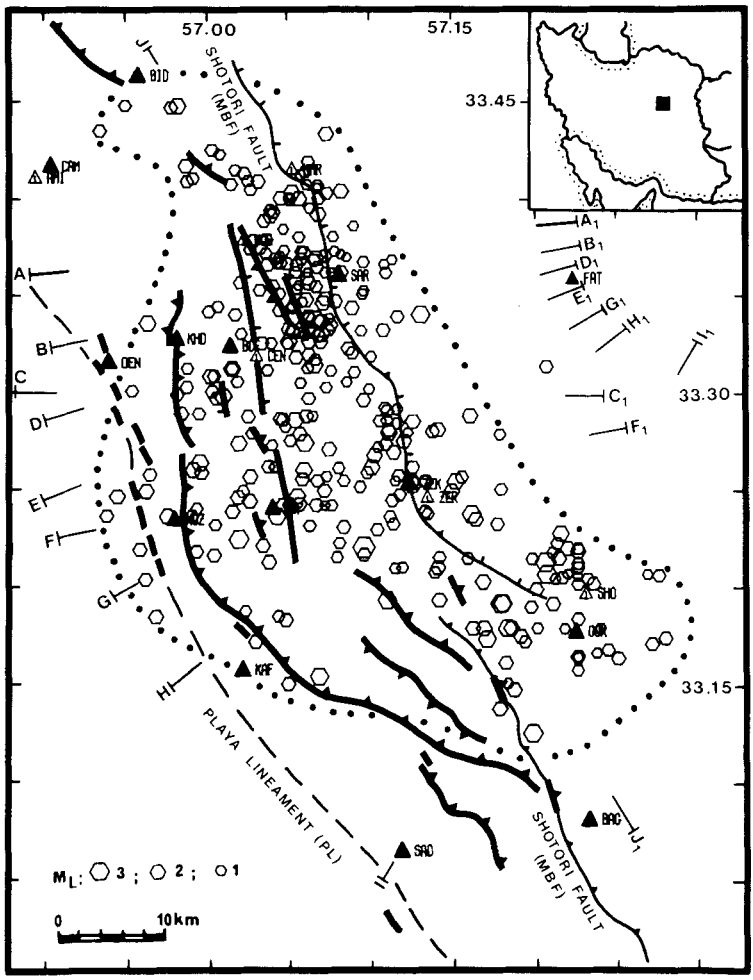

Figure 6. Epicentre map of the best-located aftershocks (329 out of 1560 events) which passed all the quality criteria (located by a single layer model). Dotted line indicates the approximate aftershock zone. Stations are shown by filled triangles, surface faulting associated with the main shock (Berberian 1979b) by a thick barbed line (triangle for thrust and short lines at right angle for high-angle reverse faults). Positions of the individual transverse and longitudinal cross-sections are shown by small lines with letters (see Fig. 7). Foothill bordering earthquake fault (FBF on cross-sections in Fig. 7) are shown by thick lines, Shotori mountain bordering reverse fault (MBF on cross-sections in Fig. 7) by a thin line, and the playa lineament (PL on cross-sections) by a dashed line. Mercator projection.

range. Complex distribution of aftershocks in a volume rather than along a simple fault plane (Fig. 13A) may indicate triggering of slip along 'several existing fault planes' within an 'imbricate thrust fault zone'.

The most striking feature of the well-located hypocentres is their apparent 'concentration' at a depth range of '8–14 km' and that the aftershock zone does not match with a single fault plane (Figs 7 and 13A). The concentration of the aftershock hypocentres at a depth range of 8–14 km could not be due to an artificial restriction in the hypocentre location or the crustal model used (see location error analyses with real (3) and synthetic data (4)). The intial depth used in the final location program was 8 km and events with a

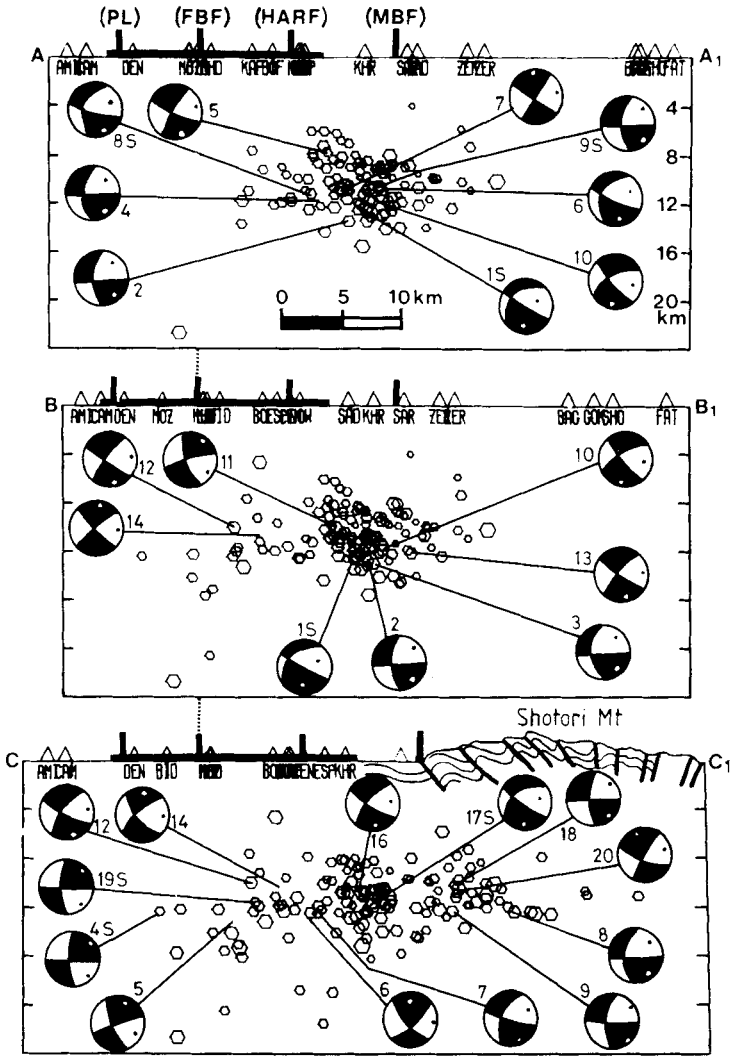

Figure 7. Vertical cross-sections of the well-located aftershocks (located by model I) of the Tabas–Shotori area with vertical (back sphere) projections of the focal mechanisms. Positions of the cross-sections, faults (thick vertical bars on top of the cross-sections), stations (triangles), and the corresponding epicentres are shown in Fig. 6. Only hypocentres within a distance of 10 km on either side of the cross-sections are plotted. Thick horizontal bars on top of the sections indicate the area of rupture at the surface developed during the main shock of 1978.09.16. Dark quadrants include compressional first motions and white dilatation. *T*-axes are plotted as open circles, and *P*-axes as solid circles. For lower hemisphere projection see Figs 9 and 10. Numbers are the same as in Figs 9 and 10. An 'S' after the number denotes a fault-plane solution for a single event. PL: Playa lineament, FBF: foothill-bordering fault (the main earthquake sole fault), HARF: high-angle reverse fault, MBF: mountain-bordering reverse fault of Shotori (for locations of these faults see Fig. 11).

fixed depth of 8 km were not chosen. Histograms showing the number of best-located aftershocks (located by three different models of I, II and III) as a function of focal depth are presented in Fig. 8. It should be noted that there is no boundary or velocity change at 8–14 km depth in the three obtained models used in this study.

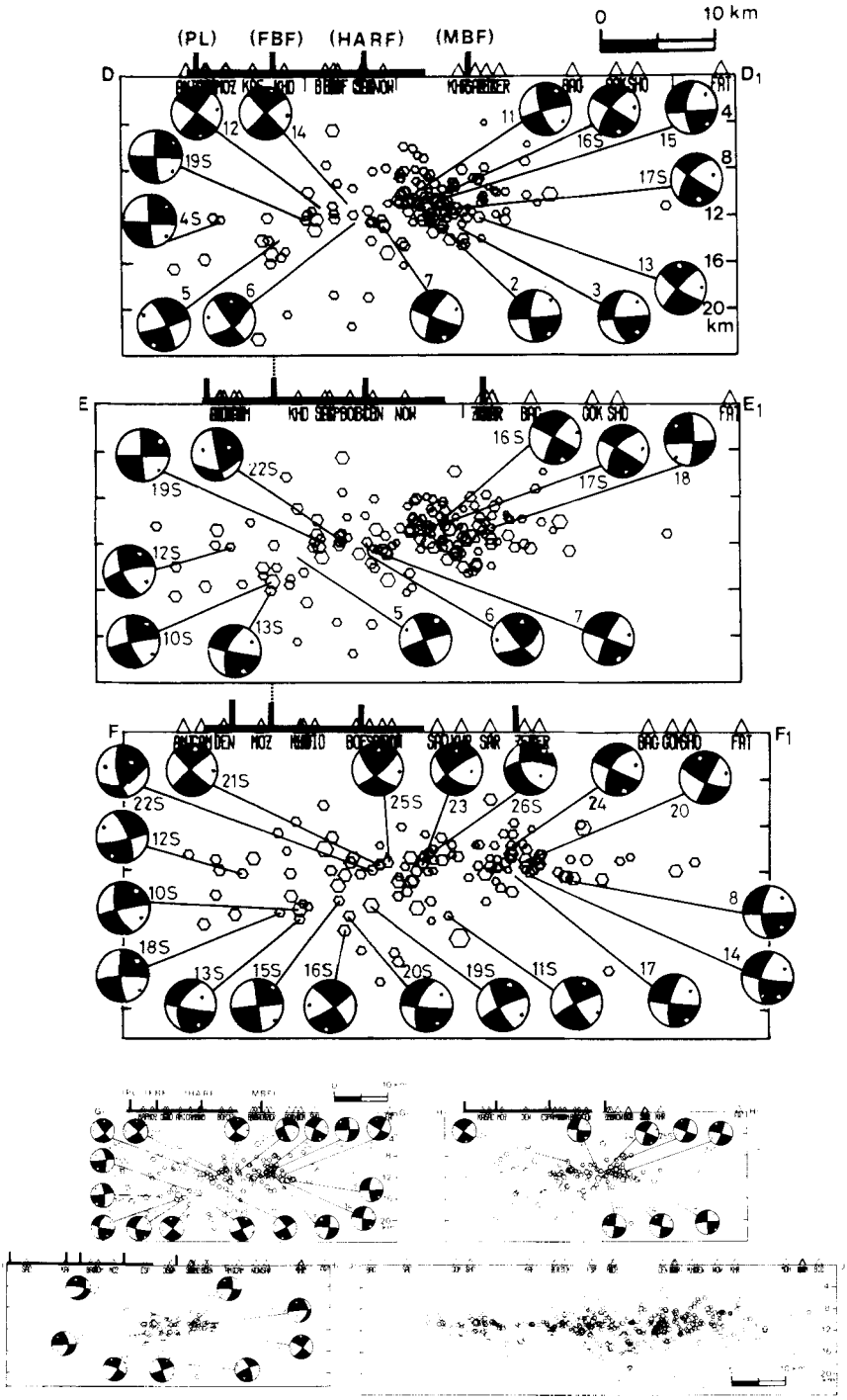

Figure 7 – *continued*

In order to correlate this high seismic zone with the regional geology, the depth ranges are compared with the accurately measured type-sections of the Shotori mountain (based on Stocklin, Eftekhar-Nezhad & Hushmandzadeh 1965 and Ruttner, Naberi & Hajian 1968):

Rock units	Thickness (km)
Tertiary	2
Mesozoic	5
Palaeozoic	8–9
Low grade metamorphics	2–4
Crystalline basement	

The Tertiary rocks together with parts of the Upper Mesozoic sediments were mostly removed by erosion from the network area, and most of the seismic stations in the Shotori mountain (i.e. east of the surface rupture) were installed on the Permian (SHO, GOK, SAR) and the Triassic (BAG, ZEK, ZER) limestone. Assuming an undisturbed sedimentary column, the thickness between the Upper Palaeozoic–Lower Mesozoic rocks and the top of the Precambrian crystalline basement seems to be around 10–13 km. This depth, which apparently coincides with the depth of the high concentration of aftershock activity (8–14 km depth), seems to be roughly at the boundary of the 'Phanerozoic Top Sedimentary Cover' and the 'Precambrian Crystalline Basement'. This coincidence may be taken to introduce a 'Decollement Zone' between the 'Cover' and the 'Basement' in the Tabas–Shotori region (Figs 7 and 13A). However, due to the considerable amount of folding and faulting, the uncertainty in the depth of the basement could not be estimated from the surface geology. The fault plane solutions of the aftershocks (Section 5.3) help to resolve this ambiguity.

The hypocentral pattern of the aftershocks shows a slight upward curving in the west towards the surface rupture zones (see cross-sections A, B, and D in Figs. 7 and 13A). Apparently this slight dip which decreases with depth is compatible with 'imbricate thrust faults' being 'listric' with decollement above the Precambrian metamorphosed basement (Figs 7 and 13A). If the listric pattern, which is introduced by the spatial distribution of the well-located aftershocks, is real, it should be documented by the well-constrained focal mechanisms (see Section 5.3). The thick seismic pattern observed in the cross-sections could

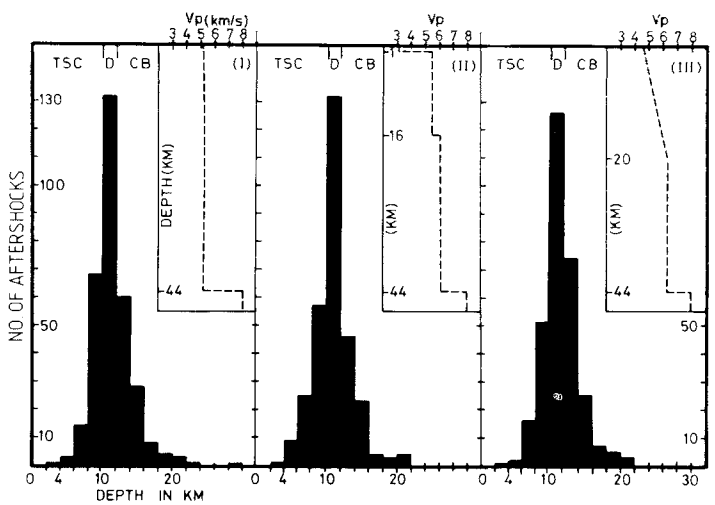

Figure 8. Histograms showing the distribution of the well-located aftershocks (with at least 5*P*- and 3*S*-readings, rms < 0.2 s, errors in epicentre and hypocentre < 2 km) as a function of focal depth, using three different models (I, II, III; shown in insets). TSC: top sedimentary cover, D: decollement, CB: crystalline basement (Precambrian) estimated from stratigraphy.

be due to 'closely spaced multiple imbricate thrusting' at depth. The hypocentral distribution of the aftershocks occurring below the zone of the high concentration, given by individual cross-sections, do not show a clear concentration (Figs 7 and 13A).

The lower level of the seismic zone (13–23 km) is probably the transition depth to ductile flow and the deeper portions of the basement thrusts are presumably shear heated and slip aseismically.

5.3 FOCAL MECHANISM SOLUTION

Since the maximum number of the portable recording stations used was usually nine, few aftershock mechanisms are well constrained. Hence composite first motion fault plane solutions were also prepared from individual solutions. The composite fault plane solutions were produced by taking each individual solution and drawing two orthogonal planes. The groups of individual solutions within an area of about 2–3 km^3 were then overlayed and a composite solution was prepared. Events with individual solutions that differed widely from a group of consistent solutions were put in a separate group. Altogether 30 individual and 30 composite fault plane solutions were prepared for the large magnitude well located aftershocks (usually larger than $M_l = 2.0$; see Figs 7 and 9–12).

A striking feature observed in the aftershock focal mechanisms is that there are 'two groups of mechanisms'. The majority of the aftershocks have a shallow ENE-dipping nodal plane, whereas a smaller group show a consistent shallow WSW-dipping nodal plane (Figs 7 and 9–12).

For most shallow aftershocks (3–12 km), one shallow ENE-dipping plane striking nearly parallel to the zone of the surface rupture was well established (Figs 7, 9 and 10). Since this plane corresponds closely to the slip surface defined by the distribution of the well-located shallow hypocentres (Figs 7, 9 and 10) and agrees with the geometry of the surface faulting, the fault plane solution of the main shock, and the regional geology, it is identified as the fault plane. The auxiliary plane is usually high angle WSW-dipping plane. Very shallow ENE-dipping to horizontal planes (Figs 7, 9 and 10) are usually located in the eastern part of the aftershock zones (far from the surface ruptures). The foci of these events are located within the depth range of 10–12 km (see Figs 7, 9 and 10). The western shallower events (i.e. closer to the surface ruptures) show steeper planes. This, together with the hypocentral pattern of the aftershocks in cross-sections A, B, C, D and H in Fig. 7, may indicate an 'imbricate listric thrust zone'. Only three solutions (Nos C11, C19S, and C26S in Fig. 9) show a steep ENE-dipping plane and a shallow WSW-dipping plane.

The sense of motion was almost 'universally thrusting' suggesting that the aftershocks and the associated tectonic deformation resulted from a relative ENE-thrusting possibly along an imbricated listric thrust zone movement which dips beneath the Shotori fold-thrust belt. Geological evidence indicates that similar overthrusting accompanied late Neogene–Quaternary mountain building phase in the region.

A large number of the deep (probably basement; 12–23 km) focal mechanisms (11 out of 25) show WSW-dipping shallow and NNE-dipping high-angle nodel planes (Figs 7 and 10). Unfortunately the spatial distribution of the deep (basement) hypocentres (Fig. 7) does not indicate which plane is the fault plane.

In order to resolve the ambiguities and to relate the seismic deformation to the observed geology and the surface faulting, the inferred fault planes, deduced from the well-constrained focal mechanisms of the well-located aftershocks, were projected on to a vertical plane (Fig. 13B). The most striking feature of this projection is a consistent deformational pattern amongst the Cover aftershocks (3–13 km depth). Fig. 13(B) clearly demonstrates an 'imbricate listric thrust fault zone' with fault planes flattening into a basement decollement

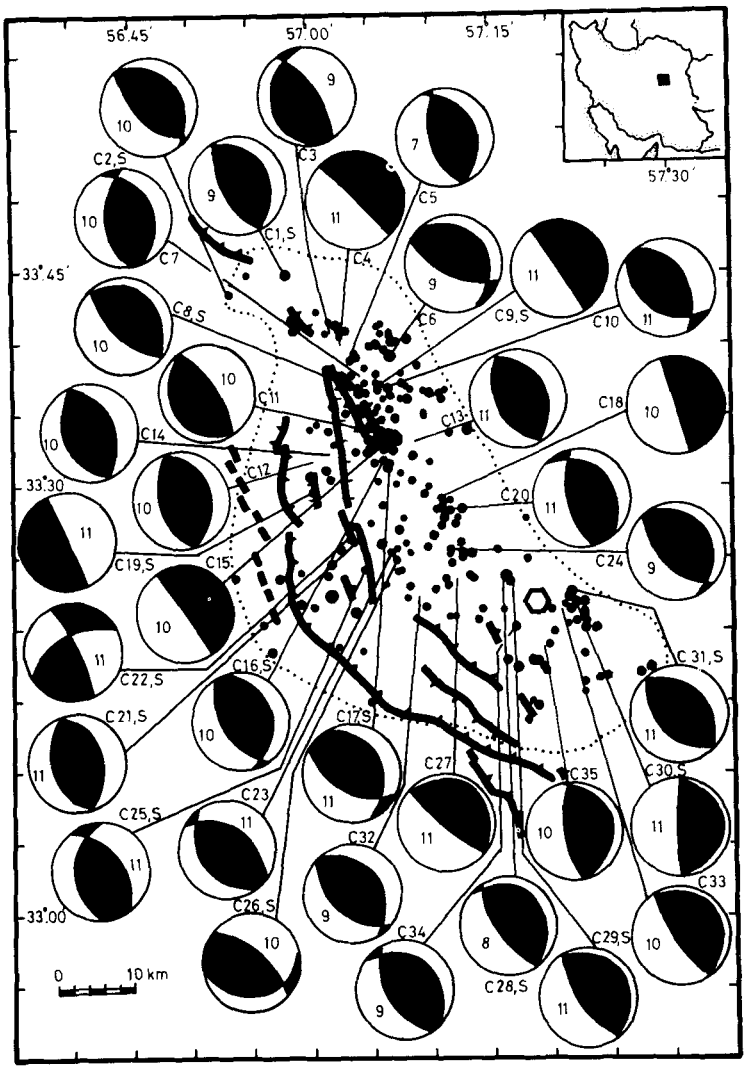

Figure 9. Focal mechanism solutions (equal-area projection of the lower focal hemisphere) of the well-located shallow (cover; h = 3–12 km) aftershocks of the Tabas-e-Golshan earthquake. An 'S' after the number denotes a fault-plane solution for a single event. For composite solutions the average location of the groups is indicated by the end of a line connected to the focal mechanisms. Numbers in the dilatational quadrants denote depth (in km). Epicentres shown are those with focal depths between 3 and 12 km. Dotted line indicates the approximate aftershock zone. The relocated main shock is shown by a hexagon. For polarity observations see Fig. 11. Seventy-two events were used to prepare 35 fault-plane solutions (15 single and 20 composite). The magnitude of the events used were ranging between M_l = 2.0 to 3.79 in 57 events and M_l = 1.51 and 2.00 in 15 aftershocks. For the vertical (back sphere) projection of the focal mechanisms see Fig. 7.

zone. Fault planes have steeper dips while approaching the surface faults in the west, whereas they flatten eastwards towards root zone of the Shotori fold-thrust mountain belt (Fig. 13B).

The spatial distribution of the well-located aftershocks (Fig. 13A) and their well-constrained focal mechanisms (Fig. 13B) clearly establish a 'decollement detachment zone' at depths between 12–13 km, which is in the range of the estimates made from the surface

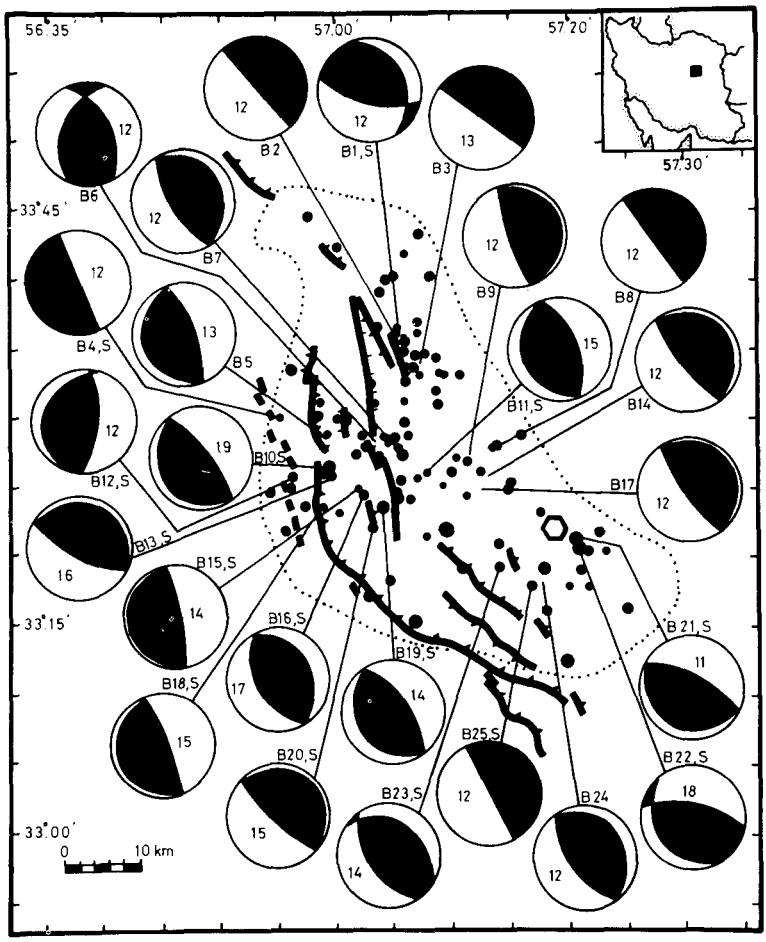

Figure 10. As with Fig. 9 but for the deep (h = 12–23 km) aftershocks. Events below 13 km depth are located in the Precambrian crystalline basement. For polarity observations see Fig. 12. Forty-two events were used to prepare 25 fault-plane solutions (15 single and 27 composite). The magnitude of the shocks used are ranging between M_l = 2.00 and 3.97 for 37 events and M_l = 1.74 and 2.00 for five events. Epicentres shown are those with focal depths greater than 12 km. For the vertical (back sphere) projection of the focal mechanism see Fig. 7.

geology (see Section 5.2). Fault plane solutions below the depth of 13 km (i.e. below the decollement zone), which falls in the Precambrian crystalline basement, show a different pattern from that of the Cover events (Figs 7, 9, 10 and 13B). This may indicate an 'independent deformation' of the basement along 'separate' reverse fault sets different from the imbricate listric thrusts of the top sedimentary cover.

Some aftershocks are located west of the main surface ruptures, on the edge of the Tabas playa (Figs 5 and 6). A similar feature was also observed during the Eshghabad (Rustanovich 1957) and the San Fernando aftershock sequences (Whitcomb *et al.* 1973). The mechanism of this pattern was never explained and the events west of the main surface rupture do not indicate the footwall deformation. The hypocentres of these events together with some other aftershocks located just east of the Tabas surface rupture and their well-constrained focal mechanisms indicate another branch of listric thrust faulting (frontal thrust belonging to the hanging-wall block) propagating west of the main fault zone (Figs 6, 7 and 13).

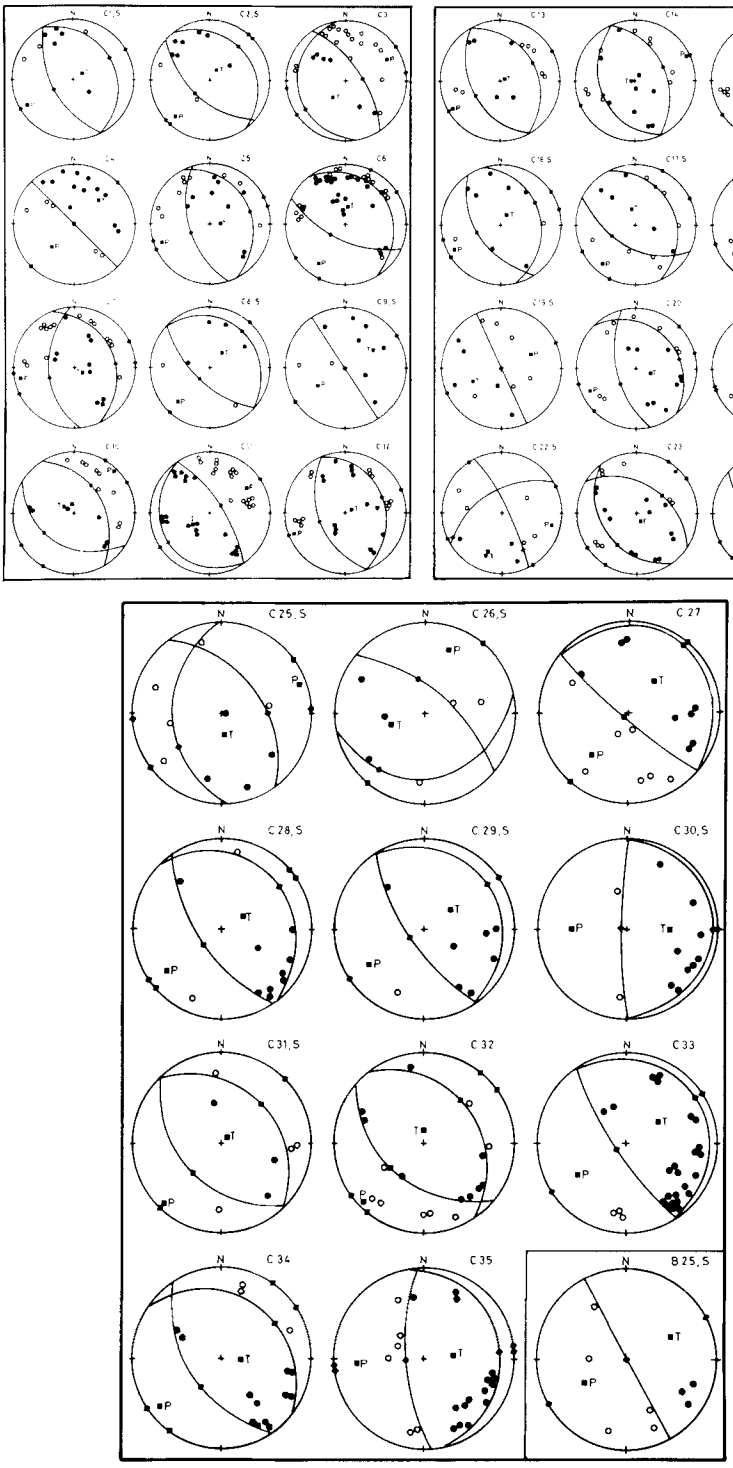

Figure 11. First motion polarity reading for the single (denoted by an S after their numbers) and the composite focal mechanism fits (equal-area projections of the lower focal hemisphere) for the well located shallow (Cover) aftershocks (h = 3–12 km). Solid circles are compressions and open circles dilatations. Numbers correspond to events in Figs 7 and 9. The horizontal projection of the slip vectors are shown by solid diamonds. T: tension axis, P: pressure axis. Event B 25, S belongs to the deep aftershocks and should be added in Fig. 12.

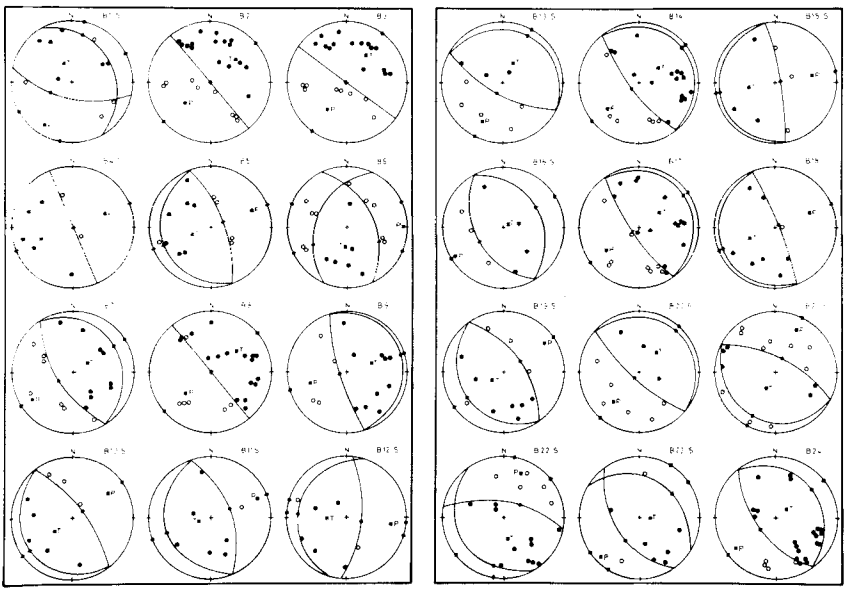

Figure 12. As with Fig. 11 but for the deep aftershocks (mostly below 12 km). Event below 13 km depth are located in the Precambrian crystalline basement. Numbers correspond to events in Figs 7 and 10. Event No. B 25, S is in Fig. 11. Data from the Iranian network are used for events B 21, S and B 22, S.

Numerous localized fractures were observed in the eastern edge of the Tabas playa, west of the main surface rupture, and some of them were mapped in the field (marked by the dashed line in Fig. 6; see also Berberian 1979b). Evidently, many zones of weakness were reactivated by the local stresses generated by the approach of the rupture front to the Earth's surface. The mapped fractures coincide with a lineament visible on the aerial photographs and *Landsat* imagery of the area, which delineate the eastern boundary of the central playa (playa lineament (PL) in Figs 6, 7 and 13).

Focal mechanism of the main shock (Fig. 1) and the aftershock sequences (Figs 7, 9 and 10) are consistent with an overall NNE continental shortening. The regional deformation observed in this study is in response to the same compressive stress system that created the present physiographical features in the Iranian plateau and agrees with the geological data for its uplift.

6 Areas of initial rupture, simplified model of faulting and aftershock tectonics

Teleseismic epicentral location of the Tabas-e-Golshan main shock given by NEIS, ISC, CSEM and MOS lies at the south-eastern end of the surface break (about 33° 22′.20″ N, 57° 26′.40″ E; see Fig. 1). The location accuracy of the post-1970 large magnitude earthquakes in Iran can be in error by 10–15 km (Berberian 1979c), but even allowing for mislocation of this amount, the approximate area of initial rupture still lies at the south-eastern end of the Tabas earthquake fault. Relocation of the main-shock epicentre using a master event technique still puts the epicentre in the southern end of the fault but moves it about 12 km towards WSW, which is within the location errors of the large magnitude Iranian earthquakes. This evidence indicates that faulting initiated near the 'southern end' of the fault (in the vicinity of 32°.22′.05″ N, 57°.18′.30″ E), presumably at a focal depth greater

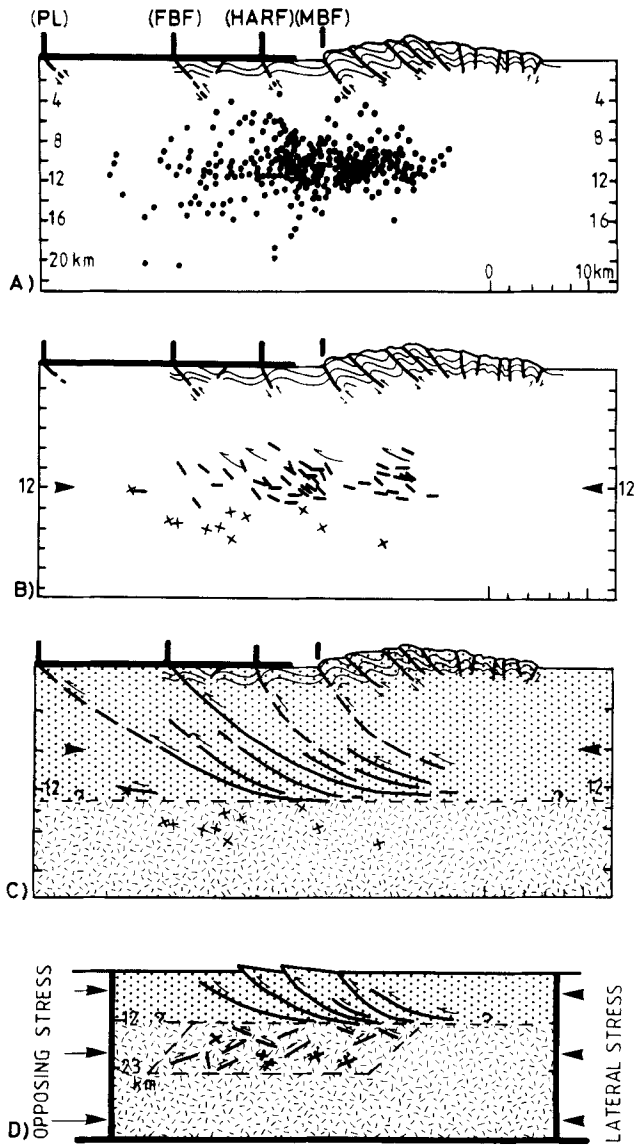

Figure 13. Deformational model of the Tabas-e-Golshan earthquake sequence along the frontal zone of the Shotori fold-thrust mountain belt. (A) Composite cross-section of the well-located aftershocks. (B) Vertical cross-sections of the inferred fault planes deduced from the well-constrained large magnitude focal mechanisms of the well-located aftershocks. Crosses indicate nodal planes of the events below the imbricate listric thrust faults (located in the Precambrian crystalline basement). (C) Relation between the seismic deformation at depth and the observed surface geology. (D) Asymmetric reverse slip deformation and plateau uplift in the top sedimentary cover rocks (stippled) above the Precambrian crystalline basement in response to lateral compression (arrows) applied to the block. Zone of high shear stress build up in the basement (due to sudden release of stress at top sedimentary cover during the main shock rupturing along a thick zone of listric faults) is shown by a parallelogram below the decollement zone. Active lateral stress (applying from right) is more than the opposing stress (left) and the results is transportation of top sedimentary cover to the left. Thick horizontal bars on top left of the cross-sections indicate the area of rupture at the surface developed during the 1978.09.16 earthquake. Positions of the reactivated faults at the surface are marked by thick vertical bars (PL – playa lineament, FBF – foothill bordering reverse fault (main earthquake fault), HARF – high angle reverse fault, MBF – mountain bordering reverse fault).

than 8 km (h = 8 km ± 2 yields the best fit to the teleseismic body-wave modelling) along the preferred fault plane striking N161°E and dipping 30° to the north-east. A fault plane dipping 30°NE through the above hypocentral position (h = 8 km) intersects the surface about 6 km east of the observed surface faulting. A plane dipping 30° NE through the surface ruptures meets the hypocentre of the main shock at depth of about 12 km.

Presumably shear failure began 'near the basement', beneath the frontal sections of the Shotori fold-thrust belt, and then propagated north-westward and upward along the main listric thrust planes to intersect the Earth's surface along the Tabas fault zone. As the fault(s) approached the free surface it splayed out into many fault segments that rupture the surface and covered a zone of about 30 km width (Fig. 13). The most striking feature of this faulting is that apparently 'several listric thrust planes' were involved (Fig. 13) and the seismic shortening did not occur on a simple fault plane. In a successive imbricate regime, the material is usually accreted on to the hanging wall, and as the fold-thrust belt moves over the decollement detachment zone, the 'frontal thrust' underlies the older ones (Dahlstrom 1970; Elliot 1976). In general, the stacking sequence in the Tabas–Shotori area is from east to west in the direction of transport and the kinematics may resemble that of an accretionary wedge formed at a subduction zone (Karig & Sharman 1975). Concentration of the Tabas aftershocks across the frontal thrust zone roughly extending from the mountain-bordering to the foothill-bordering reverse faults (MBF and FBF in Fig. 13) clearly indicates that the 'youngest sets' of the imbricate faults (frontal thrusts) in the young fold-thrust mountain belts are the 'seismically active' structures. This is supported by the fact that almost all the earthquake faults in Iran are 'frontal reverse faults' dividing young fold-thrust mountain belts from the compressional depressions (Berberian 1979b, 1981).

In response to the main-shock slippage, aftershock sequences were generated by stick-slip frictional sliding. Hypocentral locations of the best-located aftershocks and the focal mechanisms obtained in this study give a better opportunity to understand the seismotectonic evolution of recent continental deformation, than had previously been possible. The fact that the majority of the well-located Cover aftershocks (mainly events above 13 km) have mechanisms similar to that of the main shock, indicate that they occurred on the main fault zone (that slipped during the main shock) or on fault planes parallel to the main fault. Whereas slip in the basement was apparently on 'different' sets of thrust faults. Deeper events in the basement (below 13 km) show mostly a WSW-dipping shallow nodal plane (Figs 7, 9, 10 and 13). In this case Cover and Basement were reacting 'separately' to the regional compression.

Unlike the San Fernando aftershocks (Whitcomb *et al.* 1973), hypocentral distribution of the Tabas aftershocks (Fig. 13) does not show a steepening of seismic zone with depth, neither does it match with the continuation of a single surface rupture into the basement with a constant dip of 30°NE. The spatial distribution of the well-located hypocentres, however, indicate a mechanism to be offered for this region; i.e. the main shock and the aftershocks both developed along 'listric imbricate thrust faults' rooted in between the Cover–Basement boundary at depth. The deformation observed in the top sedimentary cover during this earthquake sequence is similar to that predicted by Hubbert (1951) and Hafner (1951).

The significant difference between the mechanism of the shallow (Cover) and the deep (Basement) aftershocks (with more WSW-dipping shallow planes in the latter), may indicate that after a sudden release of stress and a rapid change of the strain field by the main-shock rupturing in the lower levels of the top sedimentary cover, the value of regional shearing stress in the basement is locally increased to values sufficiently high to reactivate 'small sections' of the basement thrust faults and create the 'Secondary (Basement) aftershocks'. Due to the fast seismic strain rate, the lower levels of the basement aftershock zone has

behaved elastically. The absence of any large magnitude aftershocks in the basement may indicate that large-scale faulting did not occur in the basement. Apparently, the shear deformation within the basement is broadly distributed so that it was not possible for strain energy to accumulate to the extent necessary for a large magnitude basement earthquake to occur. Consequently, this load will be relaxed with time, again causing strain release in the intermediate crustal seismic zone. Basement aftershocks were less frequent than the Cover events and constitute about 13 per cent of the total well-located shocks (Fig. 13). During the earthquake, both the continental upper crust and the basement (to a lesser extent) underwent shortening and thickening along several reverse faults and resulted in the vertical expansion of the Shotori active fold-thrust mountain belt (Fig. 14D).

The model which is reinforced by the analyses of the well-located aftershocks and their well-constrained focal mechanisms, detailed surface mapping of the earthquake rupture and the knowledge of the regional geology and tectonics, demonstrates that the basement reactivation (secondary aftershocks) has possibly occurred 'in response' to the shortening of the top sedimentary cover. This demonstrates that when the top sedimentary cover is substantially compressed and shortened in an active decollement environment, the basement also undergoes an independent shortening and thickening.

Like other active and young mountain belts in the Iranian plateau (i.e. Zagros, Koppeh Dagh, Kuh Banan and Alborz; see Berberian 1976, 1981), the Shotori fold-thrust belt is characterized at the surface by systematic and persistent overturned or asymmetric folds amd imbricate thrust faults at the surface, with movements of overthrusting blocks to the WSW. The aftershock study revealed that the thrust faults are 'imbrications from a basal decollement' and are rooted in between the Phanerozoic sedimentary cover at the top and the Precambrian crystalline basement at depth. Structures in the sedimentary column above the Basement–Cover boundary are formed in a 'laterally moving' deformation system. Large masses of the top sedimentary cover are 'telescoped' together and moved westwards over the Precambrian metamorphic basement. It is not clear whether this detachment is a single horizontal zone, from the western Shotori fold-thrust belt to its eastern part, or together with the faults penetrates the Precambrian basement and approach a ductile shear zone at depth. The elevation differences and the eastward thickening of the thrust-stacks in the Shotori belt may indicate an east-tilting decollement horizon. However, it is clear that there was 'no' seismic activity at the 'central core' and the 'rear' part of the Shotori fold-thrust mountain belt. It is not clear how this aseismic area compensates the deformation.

The Tabas listric thrust system was probably formed by reverse movement on existing Palaeozoic (listric) normal faults. The idea is supported by contrasting lateral sedimentary facies and thickness changes on either side of the Tabas active fault set (Berberian 1979b). Over 8 km of the Palaeozoic shallow water sediments were accumulated slowly in a long, relatively narrow N–S sedimentary basin that gradually subsided along (listric ?) normal faults. The subsidence was probably an isostatic response to crustal thinning during the Palaeozoic extensional phase (Berberian & King 1981) in a manner proposed by McKenzie (1978). No major tectonic activity other than subsidence, possibly along normal faults, is recorded during this 300 Myr of the Palaeozoic stretching phase. Although the Shotori sedimentary basin did not evolve into an oceanic crust, the thickness of the Palaeozoic–early Mesozoic sediments implies that its crust was strongly stretched and thinned along normal faults at that time. The thickness of the Palaeozoic rocks within the Shotori belt of subsidence (over 8 km; Stocklin *et al.* 1965; Ruttner *et al.* 1968) is recognized here as being far greater than that of units of comparable age in the western part of the Tabas active fault zone (about 1 km; Aghanabati 1975). The following table shows thickness variations of the measured Palaeozoic and Triassic sediments in west and east of the Tabas active fault system:

Rock units	Kalmard Mt. (in the west) thickness in km	Shotori fold-thrust belt (in the east) thickness in km
Triassic	0.52	1.90
Permian	0.35	0.80
Carboniferous	0.14	1.20
Devonian	0.06	1.30
Silurian	–	0.60
Ordovician	0.40	1.20
Cambrian	–	2.30
Infracambrian	–	0.90
Low grade metamorphics		2.40
Precambrian crystalline basement		
Total thickness:	1.47	12.60

Variations in thickness (above table) and in sedimentary facies (Carboniferous gypsum in the west, shale and sandstone in the east) throughout the geological history of the region may indicate that at least some important faults like the Tabas fault system were in existence during the time of sedimentation (Fig. 14). The decollement detachment might have formed by compression which culminated in late Tertiary and continued to the Present. Telescoping of the belt and rethickening of its crust during collisional orogenies could have been carried out by a reversal of fault motion along the Palaeozoic normal faults. (Reversal of fault motion during different tensional and compressional phases is already documented on the Locris fault in Greece by Mercier (1976) and is proposed for the Shotori belt (Berberian 1979b), for the basal decollement of the Basin and Range province (Eaton 1980), for the Zagros belt (Jackson 1980; Jackson & Fitch 1981), and for the Andean foreland belt of South America (Winslow 1981).) Folding, faulting and westward displacement of the Shotori mountain belt during the collisional orogenies and their convergent movements might have 'severed' the top sedimentary structures from those at depth (Fig. 15).

Usually in the advanced fold-thrust mountain belts, such as the Rockies (Fox 1959; Price 1970, 1972, 1981; Price & Mountjoy 1970), Appalachian (King 1951, 1975; Cook *et al.* 1979; Cook, Brown & Oliver 1980; Hatcher 1981). Ouachita (King 1975), Jura (Pierce 1966), Rhenish Variscides (Meissner, Bartelsen & Mutawksi 1981), and the Moine thrust zone of the British Caledonides (McClay & Coward 1981), movement occurs by plastic deformation within the basal decollement zone of ductile materials above an unaffected basement. Apparently the Tabas–Shotori area is not involved in an advanced form of decollement tectonics simply because of the absence of basal plastic layer. Aftershocks below the zone of decollement detachment (below 13 km depth) imply that the 'Precambrian crystalline basement' as well is undergoing some 'shortening and deformation', and the top sedimentary cover is possibly still above its original basement or very close to it. The lack of real ductile beds between Basement and Cover may indicate that aseismic slip (as observed in a true detachment tectonic regime) does not play an important role in the Tabas–Shotori region, and the Basement and Cover were partly stuck together possibly along the 2–4 km of the Upper Precambrian low grade metamorphics (the low grade metamorphics are unconformably covered by the Lower Palaeozoic clastic sediments). Apparently in the case of Tabas, 'frictional drag' between Basement and Cover is 'greatly increased' because of absence of ductile beds. It could therefore be postulated that those segments of the young active

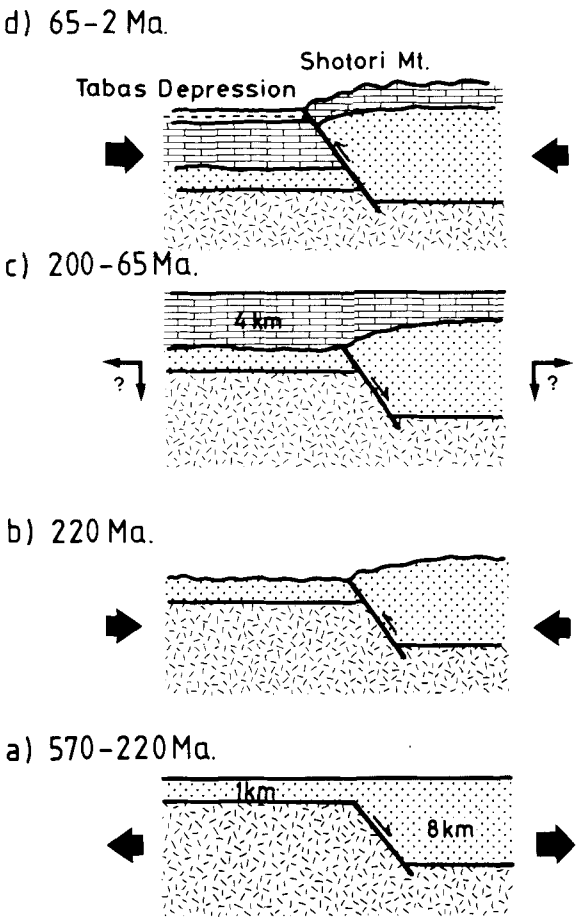

Figure 14. Stratigraphic evolution of the Tabas fault system, Tabas compressional depression and the Shotori fold-thrust mountain belt from late Precambrian to late Miocene. The compressional and tensional phases of (b) and (c) are not clearly demonstrated and sedimentation could have been controlled by eustatic changes. The depositional phase (a) and the compressional (d) are both well-established (see also the relevant tables in the text).

fold-thrust belts which lack a thick plastic layer between basement and cover (e.g. parts of the Zagros active fold-thrust belt, Alborz, Kopeh Dagh) may be involved in a similar seismic activity due to an increased frictional drag.

7 Comparison with similar (thrust) structures

Listric thrusts are usually characteristic features of most fold-thrust mountain belts, where they occur in thick sedimentary sections especially in the foreland fold and thrust belts. Listric structures (normal or reverse) are documented by different methods (laboratory experiments, geophysical exploration, drilling) in different tectonic regimes throughout the world. Recognition of 'imbricate listric thrust' and 'decollement tectonics' under the Shotori fold-thrust belt seems to be the first case revealed by detailed study of the best-located continental aftershock sequence and their well-constrained focal mechanisms in a convergent zone.

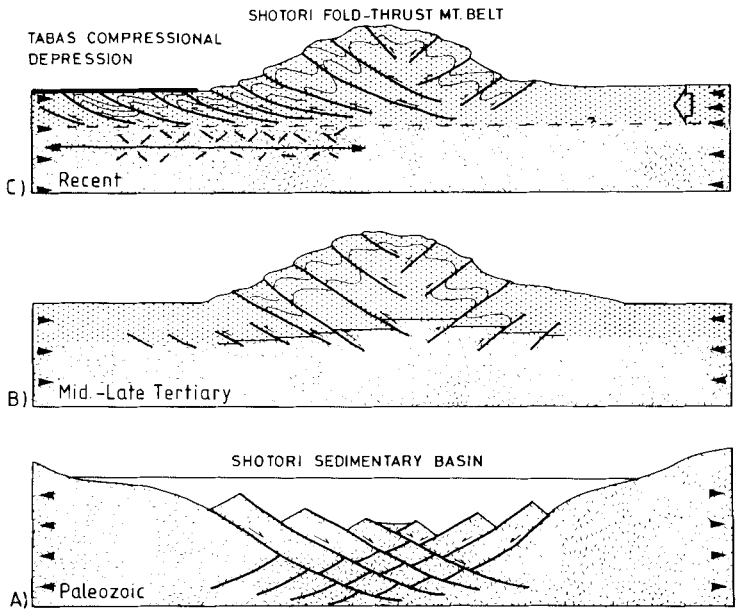

Figure 15. A possible model for structural evolution of the young Shotori fold-thrust mountain belt and the Tabas compressional depression along the Tabas active fault system. (A) Formation of the Shotori sedimentary basin by stretching and thinning of the Precambrian continental crust, development of listric normal faults and deposition of shallow water sediments during 300 Myr of the Palaeozoic extensional phase. (B) Reactivation of the old normal faults and re-thickening and shortening of the continental crust by reversal of motion during compressional phases. (C) Detachment of the top sedimentary cover from the Precambrian crystalline basement due to considerable lateral motion and development of imbricate listric thrust faults in the frontal zone of the young active fold-thrust mountain belt. The zone of 1978 seismic activity is marked by a horizontal arrow. Different active basement faults are shown by oblique lines on the horizontal arrow. Thick horizontal bar on top left of the section (in the Tabas compressional depression) indicates the area of ruptures at the surface developed during the 1978.09.16 earthquake.

The only previous study with similar scope (with thrust mechanism) was carried out after the San Fernando earthquake of 1971.02.09 (Hanks, Jordan & Minster 1971; Wesson, Lee & Gibbs 1971; Allen, Hanks & Whitcomb; Whitcomb *et al.* 1973). The San Fernando aftershock sequence revealed (a) thrust fault(s) steepening with depth. Complex volumetric distribution of aftershocks like the Point Mugu earthquake of 1973.02.21 with diverse aftershock focal mechanisms (Ellsworth *et al.* 1973; Stierman & Ellsworth 1976) and the Friuli aftershocks of the 1976.05.06 earthquake (Cagnetti & Pasquale 1979) failed to delineate any single fault plane and did not introduce a consistent or understandable deformational pattern. As with the Tabas earthquakes, aftershocks of the Inangahua (New Zealand) earthquake of 1968.05.23 ($M_0 = 7.1$, with a thrust mechanism) were distributed between 5–19 km depth with strong clustering at about 12 km depth, and no clustering was observed near the extremities of the aftershock area (Adams & Lowry 1971).

It is interesting to compare the results of the Tabas-e-Golshan aftershocks with those of the Eshghabad earthquake of 1948.10.05 (Rustanovich 1957), which is one of the earliest detailed investigations of an aftershock sequence. Although the activity was described along a NW–SE seismic line (Tchalenko 1975), the hypocentral locations indicate listric thrust fault(s) dipping southward underneath the Kopeh Dagh fold-thrust belt north-east of Iran. In both the Tabas and Eshghabad cases, the majority of aftershocks were located near the

base of the Palaeozoic at depths of 10–12 km. The 1948 Eshghabad aftershock sequence shows that aftershocks dip southwards with a flattening of the seismic zone at depth. The mountain bordering reverse faults in both cases (Shotori fault in Tabas, see Fig. 6, and the Main Kopeh Dagh reverse fault in Eshghabad; see Berberian 1981) were not reactivated at the surface (there was no direct connection between the Eshghabad earthquake of 1948 and the Main Kopeh Dagh fault zone; see Rustanovich & Shirokova 1964 and Tchalenko 1975 for discussion). In the case of Tabas, surface ruptures were developed along the foothill-bordering reverse faults and were associated with the area of the maximum intensity. During the Eshghabad earthquake no surface faulting was observed along the foothills (except some ruptures at Kuru Gaudan; Kopp, Rastsvetaev & Trifonov 1964; Gorshkov & Yakushova 1967), but the detailed isoseismal map shows the maximum intensity elongated along the foothills border zone. This may indicate that the earthquake rupture did not propagate towards the surface possibly due to the presence of some ductile beds in the Kopeh Dagh belt, whereas there is no major bed in the Tabas–Shotori area.

8 General discussion and conclusion

The Tabas-e-Golshan earthquake sequence of 1978 September–October was examined in detail to investigate the active continential deformation in a young fold-thrust mountain belt which is currently shortening and thickening. The main shock of 1978.09.16 (M_S = 7.4) was associated with 85 km of discontinuous surface faulting along an existing but hitherto unrecognized late Quaternary frontal reverse fault of Tabas. Extensive zone of bedding-plane slip with thrust mechanism were also developed in the hanging-wall block, indicating an extensive hanging-wall deformation.

Detailed analyses of the surface fault breaks, fault-plane solution of the main shock and of the aftershocks, showed that the earthquake was caused by movement of ENE-dipping thrust fault(s) at the base of the frontal segment (foothills) of a young fold-thrust mountain belt (the Shotori mountains), and conforms with the deformation pattern within the belt. The overall fault motion was thrusting of the Shotori fold-thrust belt from ENE over the Tabas depression in the WSW. The mountain-depression structure was formed during compressional phases in the post-Neogene–early Quaternary time along mountain-bordering reverse faults.

The Tabas foothill reverse fault system seems to be one of the principal structures by which the western flank of the Shotori fold-thrust mountain belt is raised about 2 km above the Quaternary alluvial deposits of the Tabas compressional depression. Geological data indicate that the Tabas fault system is possibly a 'multi-role deep-seated Precambrian structure' and one of the major features during the Palaeozoic and the Mesozoic extensional phases in the western part of the fault-controlled subsiding sedimentary basin of Shotori. A comparison of the Plio-Pleistocene and late Quaternary crustal deformation associated with this earthquake indicated that the earthquake is a clear case of fault reactivation and continuation of the late Alpine compressional tectonic regime.

Locally recorded aftershock sequences of the 1978 Tabas-e-Golshan earthquake were located using three velocity models. A series of tests were used to evaluate different sources of uncertainty, and a quality criterion was developed for estimating the precision of the locations of the aftershocks. Out of 1560 located events only 329 good locations were obtained. These well-located aftershocks, which have uncertainties in epicentre and in focal depth of about 1 and 2 km respectively, provided detailed picture of seismic deformation. The 329 well-located aftershocks together with their well-constrained focal mechanisms were used to correlate the aftershock activity with the geological structures and with the surface faulting which accompanied the main shock of 1978.09.16.

Almost all the well-located aftershocks lie to the east of the mapped surface ruptures, presumably on thrust planes dipping ENE, and indicate an 'intense hanging-wall deformation'. The epicentral pattern has an arcuate shape and follows very closely the pattern of the earthquake faults at the surface.

The most striking feature of the well-located hypocentres is that the aftershock zone does not match with a single fault plane having a constant dip of 30°NE from the surface to the basement (fault dip measured at the surface and obtained from the focal mechanism of the main shock). The hypocentres occurred mainly at depths less than 23 km with a high concentration of seismic activity between 8–14 km depth, indicating a 'decollement zone' between the Phanerozoic top sedimentary cover and the Precambrian crystalline basement. The hypocentral distribution together with the focal mechanisms suggest reactivation of an 'imbricate listric thrust zone' at top sedimentary cover.

The thick seismic zone and its complicated pattern along the frontal zone of the young Shotori fold-thrust belt, is a geometrical consequence of motion on imbricate reverse listric faults. It is observed that the imbricate thrust faults at the surface are imbrications from a basal decollement detachment. The shallow events (3–13 km depth) have fault plane solutions similar to that of the main shock. This indicates that the aftershock sequence contributed to a continued slip on fault system similar and/or parallel to the main-shock fault plane(s). Events located between 10–13 km depth commonly have one nodal plane which is either horizontal or has a shallow dip, whereas many deep shocks (below 13 km) are characterized by WSW-shallow dipping nodal planes. The basement aftershocks are considered here as 'secondary events' induced by and in response to a considerable shortening of the top sedimentary cover. Faults in the basement were reactivated as a consequence of the sudden release of stress at the top sedimentary cover along a thick zone of imbricate listric thrust faults. The study illustrated that both the upper crust and the basement underwent crustal shortening and thickening during this earthquake sequence.

Hypocentral distribution of the best-located aftershocks, together with their focal mechanisms, revealed a consistent deformation pattern in the top sedimentary cover. The hypocentral pattern and the large variety in the dips of the nodal planes in the Cover and the Basement aftershock mechanisms reflect a complicated mode of seismic deformation and indicates that more than one fault system was reactivated in the Cover and the Basement. In response to the shortening of the top sedimentary cover, basement faults were also reactivated. The average width of the zone of the aftershock hypocentres (about 30 km) matches with the zone of the surface faulting. This may indicate that most parts of the seismic zone at depth propagated to the surface.

Detailed study of the well-located aftershocks and the focal mechanisms provided an answer to the question about the behaviour of the crystalline basement when the top sedimentary cover is substantially shortened and telescoped above it. The Tabas aftershock data revealed that the basement experienced shortening and thickening, and that it did not remain a rigid or inactive lithosphere during a continental earthquake. The active tectonics style of the young Shotori fold-thrust belt is characterized by frontal listric thrust imbrication, distant transport of the top sedimentary cover over a decollement detachment zone, and deformation of Precambrian crystalline basement. The kinematics of the top sedimentary cover resemble that of a tectonically thickened accretionary wedge formed at a subduction zone. Listric reverse faults throughout the Shotori fold-thrust mountain belt seems to be geometrically related to folding. The faults are responsible for a large percentage of the crustal shortening within the cover rocks by imbrication of thrust slices.

The study provided a clear picture of active continental deformation in a young fold-thrust mountain belt and indicated that development of young fold-thrust belts during orogenic processes 'necessarily involves basement shortening'. Similar Shotori-type 'thin- and

thick-skinned tectonic' deformation may prevail in other young and active fold-thrust mountain belts characterized by a thick sequence of telescoped top sedimentary cover over a decollement zone.

The active tectonic style and mode of deformation of the Shotori fold-thrust belt are, thus, particularly different from those observed in thin- or thick-skinned tectonics (Rodgers 1949, 1953). Apparently it is the first documented active 'Cover–Basement deformation' case with both 'thin- and thick-skinned tectonics' affinities. Its deformational pattern could not be regarded as typical thin-skinned tectonics since the basement was also involved in active shortening and thickening. Neither could it be categorized as typical thick-skinned tectonics because the Cover faults and the fold-thrust mountain belt were decoupled from the original underlying basement during westward transportation of the top sedimentary cover over the decollement zone.

The Tabas-e-Golshan seismic activity is a small part of the diffuse seismic pattern in the Iranian plateau. The 'scattered seismic pattern' in most parts of the Iranian continental crust (see Berberian 1976, 1979b, 1981) may be due to the fact that the crust consists of an agglomeration of different continental fragments separated from the Arabian shield and accreted to Eurasia (Berberian & King 1981). Apparently in this crust some older and stronger Precambrian shield-like cores have not remobilized during the younger deformational phases and resisted deformation; although they were subject to the same forces as the adjacent mobile belts. Apparently compressional stresses can be transmitted laterally through the crust of the more rigid blocks to the mobile belts (i.e. mountain-bordering reverse faults). Comparison of the pre-Quaternary and the recent continental deformation indicates that the present activity is the continuation of the long-established tectonic regime that has resulted in the uplifting of the mobile fold-thrust mountain belts along 'frontal (listric) reverse faults', and downthrusting of possibly more rigid blocks which are not deformed (apparently represented by some compressional depressions). The difference in elevation between the compressional depressions and the bordering active fold-thrust mountain belts is possibly caused by differences in crustal structure and a reversal of fault motions during a dominant compressional tectonic regime.

The seismic activity is mainly concentrated along the 'frontal reverse faults' of the mobile belts (mountain-front and foothill thrusts), and earthquake faulting follows exactly the obvious fault scarps created by the late Quaternary faulting. These frontal active reverse faults are the 'youngest sets of imbricate thrusts' in the young fold-thrust mountain belts, and have been reactivated extensively during the late Alpine orogenic phases.

In this study a detailed three-dimensional structure of an active fault zone situated in front of a young fold-thrust mountain belt was determined using the locations and focal mechanisms of the well-located aftershock sequence. It is demonstrated that the aftershocks shared the same tectonic causes as the main shock, and that the decollement tectonics in active fold-thrust belts may involve the upper levels of the crystalline basement.

Acknowledgments

Many fruitful discussions with Dan McKenzie, Chris Scholz, James Jackson, Bruce Bolt, Isa Asudeh, Chris Soufleris, Alan Smith, Geof King, Harsha Sinvhal, Alistair Sharp, Carl Spencer and their comments, corrections and suggestions are greatly appreciated.

The aftershock recording and earthquake fault mapping took place over 40 days in the field. The smoked-drum recording instruments were on loan from the Lamont-Doherty Geological Observatory of the Columbia University, Department of Geophysics, Imperial College, London and Laboratoire Seismologique, Universite de Paris-sud, Centre d'Orsay.

The Department of Geophysics, Ferdowsi University of Mashhad, provided two more instruments which were operated during the last 16 days of the field study.

The 40-day field expedition would not have been possible without enthusiastic cooperation from the Geological and Mineral Survey of Iran (especially R. Assefi, Managing Director and J. Eftekharnezhad, Deputy Manager), which provided all the field support. Additional support for the aftershock project was received from the Natural Environment Research Council (UK), the Royal Society of Great Britain, the Carnegie Institute (UK), consulting work of myself and Geof King for the Spencer and Partners Consulting Engineers London (on the seismotectonic investigation of the Pars Trunk pipeline in Zagros) and the United States Geological Survey.

Chris Scholz and Roger Bilham from the Lamont-Doherty Geological Observatory of the Columbia University assisted with the first phase of the aftershock recording project and provided valuable discussions in the field. I am gratefully to Isa Asudeh and Chris Soufleris for their very friendly help during the aftershock recording stage in a very difficult expedition and desert climate. Mash Jafar (cook), Kazemzadeh, Julai and Rahemi (drivers), Dehghan (technician) and Behruz are acknowledged for their cooking, driving and great help during a continuous 40 days of overtime working in the desert. Graham Yielding digitized one-third of the aftershock data and the rest was digitized by myself. Gratitude is also expressed to the Department of the Armenian Affairs of the Galuste Gulbenkian Foundation (Lisbon), Education Department of the American Vicarage, London (Rt Rev. Bishop Nerises Bozabalian), British Petroleum and British IBM for donating separate small grants during the course of this research. Cambridge Earth Sciences Contribution No. ES 161.

I am deeply sorry and depressed for 20 000 innocent people who lost their lives during this unpleasant shaking of mother Earth. I hope governments in the seismically and politically active regions will seriously think about the lives of the people and will start enforcing aseismic codes and helping the villagers by financial assistance.

References

Adams, R. D. & Lowry, M. A., 1971. The Inangahua earthquake sequence, 1968, in *Recent Crustal Movements* eds Collins, B.W. & Fraser, R., *Bull. R. Soc. N.Z.*, **9**, 129–135.

Aghanabati, A., 1975. Etude geologique de la region de Kalmard (W. Tabas): stratigraphique et tectonique, *thesis*, Grenoble, 231 pp. (and 1977, *Geol. Min. Surv. Iran*, **35**).

Akasheh, B., 1975. Travel time residuals in the Iranian plateau, *J. Geophys.*, **41**, 281–288.

Akasheh, B. & Eshghi, I., 1980/81. The Tabas (Iran) earthquake of 16 September 1978, *Pageoph.*, **119**, 207–211.

Allen, C. R., Hanks, T. C. & Whitcomb, J. H., 1973. San Fernando earthquake: seismological studies and their tectonic implications, in San Fernando, California, earthquake of February 9, 1971, *USDC/NOSS*, **III**, 13–21.

Arkhangl'skaya, M., Gergaui, A. & Shechkov, B. I., 1974. On the structure of the Earth's crust in the regions of the Arabian peninsula and the Iranian highland according to surface-wave dispersion, *Izv. Earth Phys.*, **9**, 60–66.

Berberian, M., 1976. Contribution to the seismotectonics of Iran (part II), *Geol. Surv. Iran*, **39**, 7–141.

Berberian, M., 1979a. Tabas-e-Golshan (Iran) catastrophic earthquake of 16 September 1978; a preliminary field report, *Disaster*, **2**, 207–219.

Berberian, M., 1979b. Earthquake faulting and bedding-thrust associated with the Tabas-e-Golshan (Iran) earthquake of September 16, 1978, *Bull. seism. Soc. Am.*, **69**, 1861–1887.

Berberian, M., 1979c. Evaluation of the instrumental and relocated epicentres of the Iranian earthquakes, *Geophys. J. R. astr. Soc.*, **58**, 625–630.

Berberian, M., 1981. Active faulting and tectonics of Iran, *Am. Geophys. Un. Geodynam. Ser. WG6*, submitted.

Berberian, M., Asudeh, I., Bilham, R. G., Scholz, C. H. & Soufleris, C., 1979. Mechanism of the main shock and the aftershock study of the Tabas-e-Golshan (Iran) earthquake of September 16, 1978: a preliminary report, *Bull. seism. Soc. Am.*, **69**, 1851–1859.

Berberian, M. & King, G. C. P., 1981. Towards a paleography and tectonic evolution of Iran, *Can. J. Earth Sci.*, **18**, 210–265.

Bolt, B. A., Kubo, P. O. & Uhrhammer, R. A., 1978. Optimum station distribution of hypocentres for small seismographic networks. Seismographic Station, Univ. California, Berkeley, California, *Misc. Paper S-78-9.*

Cagnetti, V. & Pasquale, V., 1979. The earthquake sequence in Friuli, Italy, 1976, *Bull. seism. Soc. Am.*, **69**, 1797–1818.

Cook, F. A., Albaugh, D. S., Brown, L. D., Kaufman, S., Oliver, J. E. & Hatcher, Jr, R. D., 1979. Thin-skinned tectonics in the crystalline southern Appalachian; COCORP seismic-reflection profiling of the Blue Ridge and Piedmont, *Geology*, **7**, 563–567.

Cook, F. A., Brown, L. D. & Oliver, J. E., 1980. The southern Appalachians and the growth of the continents, *Sci. Am.*, **243**, 124–138.

CSEM. Centre Seismologique Europeo-Mediterraneen, Strasbourg, France.

Dahlstrom, C. D. A., 1970. Structural geology in the eastern margin of the Canadian Rocky Mountains, *Bull. Can Petrol. Geol.*, **18**, 332–406.

Eaton, G. P., 1980. Geophysical and geological characteristics of the crust of the Basin and Range province, in *Studies in Geophysics; Continental Tectonics*, pp. 96–113, National Academy of Sciences, Washington, DC.

Elliott, D., 1976. The motion of thrust sheets, *J. geophys. Res.*, **81**, 949–963.

Ellsworth, W. L., Campbell, R. H., Hill, D. P., Page, R. A., Alewine III, R. W., Hanks, T. C., Heaton, T. H., Hileman, J. A., Kanamori, H., Minster, B. & Withcomb, J. H., 1973. Point Mugu, California, earthquake of 21 February 1973 and its aftershocks, *Science*, **182**, 1127–1129.

Fox, F. G., 1959. Structure and accumulation of hydrocarbons in southern foothills, Alberta, Canada, *Bull. Am. Ass. Petrol. Geol.*, **43**, 992–1025.

Francis, T. J. G., Porter, I. T., & McGrath, J. R., 1977. Ocean-bottom seismograph observations on the Mid-Atlantic Ridge near lat. 37N, *Bull. geol. Soc. Am.*, **88**, 664–677.

Gorshkov, G. P. & Yakushova, A. F., 1967. The Ashkhabad earthquake of October 6, 1948, in *Physical Geology*, chapter 16, (1), 437–441, Mir Publ., Moscow.

Hafner, W., 1951. Stress distribution and faulting, *Bull. geol. Soc. Am.*, **62**, 373–398.

Hanks, T. C., Jordan, T. H. & Minster, J. B., 1971. Precise locations of aftershocks of the San Fernando earthquake 2300 (GMT) February 10–1700 February 11, 1971, *Prof. Pap. US geol. Surv.*, **733**, 21–23.

Hatcher, Jr, R. D., 1981. Thrust and nappes in the North American Appalachian orogen, in *Thrust and Nappe Tectonics*, eds McClay, K.R. & Price, N.J., *Spec. Publ. geol. Soc. Lond.*, **9**, 491–499, Blackwell Scientific Publications, Oxford.

Hubbert, M. K., 1951. Mechanical basis for certain familiar geologic structures, *Bull. geol. Soc. Am.*, **62**, 355–372.

ISC. Bulletin of the International Seismological Centre, Edinburgh, Scotland.

Jackson, J. A., 1980. Reactivation of basement faults and crustal shortening in orogenic belts, *Nature*, **283**, 343–346.

Jackson, J. & Fitch, T., 1981. Basement faulting and the focal depths of the larger earthquakes in the Zagros mountains (Iran), *Geophys. J. R. astr. Soc.*, **64**, 561–586.

Karig, D. E. & Sharman, G. E., 1975. Subduction and accretion in trenches, *Bull. geol. Soc. Am.*, **86**, 377–389.

King, P. B., 1951. *The Tectonics of Middle North America*, Princeton University.

King, P. B., 1975. The Ouachita and Appalachian orogenic belts, in *The Ocean Basins and Margins, 3, The Gulf of Mexico and the Carribean*, eds Nairn, A. E. & Stehli, F. G., Plenum Press, New York.

Kopp, M. L., Rastsvetaev, L. M. & Trifonov, G., 1964. Tectonicheskie treshiny, obrazovavshieisia pri golotsenovyh zemletriaseniakh tsentral'novo Kopt–Daga i evo predgory, *Izv. Akad. Nauk SSSR (ser Geol.)*, 7, 59–69.

Lee, W. H. K. & Lahr, J. C., 1975. HYPO-71 (revised): a computer program for determining hypocenter, magnitude and first motion pattern of local earthquakes, *SGS Open File Rep.*, pp 75–311.

McClay, K. R. & Coward, M. P., 1981. The Moine Thrust Zone. An overview, in *Thrust and Nappe Tectonics*, eds McClay, K.R. & Price, N.J., *Spec. Publ. geol. Soc. Lond.*, **9**, 241–260, Blackwell Scientific Publications, Oxford.

McCowan, D. W., 1978. High-resolution group velocity analysis, *Geoexplor.*, **16**, 97–109.

McKenzie, D. P., 1978. Some remarks on the development of sedimentary basins, *Earth planet. Sci. Lett.*, **40**, 25–32.

Meissner, R. B., Bartelsen, H. & Mutawski, H., 1981. Thin-skinned tectonics in the northern Rhenish Massif, Germany, *Nature*, **290**, 399–401.

Mercier, J. L., 1976. La neotectonique, ses methodes et buts. Un example: l'arc Egian (Mediterranee orientale), *R. Geogr. Phys. Geol. Dyn. (2)*, **XVIII**, 323–346.

Moazami-Goudarzi, K., 1974. La vitesse de phase des ondes de Rayleigh et les structures de la croute et du manteau superieur entre Machhad et Chiraz (Iran), *Pageoph.*, **112**, 675–681.

Mohajer-Ashjai, A. & Nowroozi, A. A., 1979. The Tabas earthquake of September 16, 1979 in east-central Iran, a preliminary field report, *Geophys. Res. Lett.*, **6**, 689–692.

MOS, Moscow, Institute of Physics of the Earth, USSR.

Nason, R., 1973. Increased seismic shaking above a thrust fault, in *San Fernando, California, earthquake of February 9, 1971*, **III**, 123–126, NOAA, Washington, DC.

NEIS. National Earthquake Information Services. *Preliminary Determination of Epicentres, Monthly Listing*, US Geological Survey.

Nur, A. & Simmons, G., 1969. The effect of saturation on velocity in low porosity rocks, *Earth planet. Sci. Lett.*, 7, 183–193.

Nuttli, O. W., 1980. The excitation and attenuation of seismic crustal phases in Iran, *Bull. seism. Soc. Am.*, **70**, 469–487.

Peive, A. & Yanshin, A. L. (eds), 1979. *Scheme of distribution of continental crusts of various ages in northern Eurasia and relief of the Moho surface scale 1:5,000,000*, Geological Institute, USSR.

Pierce, W. G., 1966. Jura tectonics as a decollement, *Bull. geol. Soc. Am.*, 77, 1265–1276.

Plafker, G., 1972. Tectonics of the March 27, 1964, Alaska earthquake, in *The Great Alaska Earthquake of 1964, Seismology and Geodesy*, pp. 113–188, National Academy of Sciences, Washington, DC.

Price, R. A., 1970. Structure of the southern Canadian Cordillera. *Spec. Pap. geol. Ass. Can. 6.*

Price, R. A., 1972. Tectonics and structural geology in Canada, *Earth Sci. Rev.*, **8**, 137–138.

Price, R. A., 1981. The Cordilleran foreland thrust and fold belt in the southern Canadian Rocky Mountains, in *Thrust and Nappe Tectonics*, eds McClay, K.R. & Price, N.J., *Spec. Publ. geol. Soc. Lond.*, **9**, 427–448, Blackwell Scientific Publications, Oxford.

Price, R. A. & Mountjoy, E. W., 1970. Geological structure of the Canadian Rocky mountains between Bow and Athabasca rivers – a progress report, in *Structure of the Southern Canadian Cordillera*, ed. Wheeler, J. O., *Spec. Pap. geol. Ass. Can.*, **6**, 7–25.

Rodgers, J., 1949. Evolution of thought on structures of middle and southern Appalachians, *Bull. Am. Ass. Petrol. Geol.*, **33**, 1643–1654.

Rodgers, J., 1953. The folds and faults of the Appalachian Valley and ridge province. Southern Mineral Symposium, 1950, *Spec. Publ. Kentucky Geol. Surv. ser. 9*, **4**, 150–166.

Rustanovich, D. N., 1957. Some problems of the investigations of the seismic activity of the Ashkhabad region, *Izv. Akad. Nauk SSSR (ser Geofiz)*, **1**, 9–21.

Rustanovich, D. N. & Shirokova, E. I., 1964. Some results of the study of the Ashkhabad earthquake of 1948, *Izv. Akad. Nauk SSSR (ser Geofiz.)*, **12**, 1077–1080.

Ruttner, A., Nabavi, M. H. & Hajian, J., 1968. Geology of the Shirgesht area (Tabas area, East Iran), *Geol. Surv. Iran*, **4**, 133 pp.

Sharp, R. & Orsini, N. A., 1978. Preliminary report on the Tabas, Iran earthquake of September 16, 1978, *Earthquake engr. Res. Inst. Newsl.*, **12**, 30–34.

Stierman, D. & Ellsworth, W. L., 1976. Aftershocks of the February 21, 1973 Point Mugu, California earthquake, *Bull. seism. Soc. Am.*, **66**, 1931–1952.

Stocklin, J., Efterkhar-Nezhad, J. & Hushmandzadeh, A., 1965. Geology of the Shotori Range (Tabas area, East Iran), *Geol. Surv. Iran*, **3**, 69 pp.

Tchalenko, J. S., 1975. Seismicity and structure of the Kopet Dagh (Iran, USSR), *Phil. Trans. R. Soc. A*, **278**, 1–28.

Uhrhammer, R. A., 1980. Observations of the Coyote Lake. California earthquake sequence of August 6, 1979, *Bull. seism. Soc. Am.*, **70**, 559–570.

Wesson, R. L., Lee, W. H. K. & Gibbs, J. F., 1971. Aftershocks of the San Fernando earthquake, *Prof. Pap. U.S. geol. Surv.*, **733**, 24–29.

Whitcomb, J. H., Allen, C. R., Garmany, J. D. & Hileman, J. A., 1973. San Fernando earthquake series, 1971: focal mechanisms and tectonics, *Rev. Geophys. Space Phys.*, **11**, 693–730.

Winslow, M. A., 1981. Mechanisms for basement shortening in the Andean foreland fold belt of southern South America, in *Thrust and Nappe Tectonics*, eds McClay, K.R. & Price, N.J., *Spec. Publ. geol. Soc. Lond.*, **9**, 513–528, Blackwell Scientific Publications, Oxford.